Henri Jussila

Fabrication of Indium Arsenide Quantum Dot Structure for Semiconductor Optical Amplifiers

Faculty of Electronics, Communications and Automation

Thesis submitted for examination for the degree of Master of Science in Technology.

Espoo 30.3.2010

Thesis supervisor:

Prof. Markku Sopanen

Thesis instructors:

Doc. Teppo Hakkarainen

Dr. Abuduwayiti Aierken

Aalto University
School of Science
and Technology

AALTO UNIVERSITY
SCHOOL OF SCIENCE AND TECHNOLOGY

ABSTRACT OF THE
MASTER'S THESIS

Author: Henri Jussila

Title: Fabrication of Indium Arsenide Quantum Dot Structure for Semiconductor Optical Amplifiers

Date: 30.3.2010 Language: English Number of pages:7+41

Faculty of Electronics, Communications and Automation

Department of Micro- and Nanotechnology

Professorship: Optoelectronics Code: S-104

Supervisor: Prof. Markku Sopanen

Instructors: Doc. Teppo Hakkarainen, Dr. Abuduwayiti Aierken

In this thesis, the properties of self-assembled InAs/InGaAsP/InP quantum dots (QD) have been investigated. The focus of this work was to fabricate such a structure that can be used in a telecommunication wavelength semiconductor optical amplifier (SOA). The examined InAs QD samples were fabricated by metalorganic vapor-phase epitaxy technique. Photoluminescence (PL) and atomic force microscopy (AFM) were used in the characterization of the optical and the structural properties of the samples, respectively. InAs island size and the areal density was first optimized for SOAs by growing self-assembled InAs islands directly on InP. These results were used to finalize the structure containing also InGaAsP waveguide layer. The AFM results of the final structure show that InAs islands were grown quite homogenously on InGaAsP with an average height of 10 nm and an average base diameter of 30 nm. The low temperature PL peak of InAs/InGaAsP/InP quantum dots was tuned to 1.56 μm wavelength.

Keywords: Indium phosphide, indium arsenide, indium gallium arsenide phosphide, quantum dot, semiconductor optical amplifier, metalorganic vapor phase epitaxy.

AALTO-YLIOPISTO
TEKNILLINEN KORKEAKOULU

DIPLOMITYÖN
TIIVISTELMÄ

Tekijä: Henri Jussila

Työn nimi: Indiumarsenidikvanttipisterakenteen valmistaminen optiseen puolijohdevahvistimeen

Päivämäärä: 30.3.2010 Kieli: Englanti Sivumäärä:7+41

Elektroniikan, tietoliikenteen ja automaation tiedekunta

Mikro- ja nanotekniikan laitos

Professuuri: Optoelektroniikka Koodi: S-104

Valvoja: Prof. Markku Sopanen

Ohjaajat: Dos. Teppo Hakkarainen, Tkt. Abuduwayiti Aierken

Tämä diplomityö tutkii itseorganisoidusti valmistettuja InAs kvanttipisteitä InGaAsP:n ja InP päällä. Työn tavoitteena on ollut sellaisen kvanttipisterakenteen valmistaminen, joka soveltuu optiseen puolijohdevahvistimeen (SOA) tietoliikenneaallonpituuksilla. Työtä varten valmistettiin InAs-kvanttipistenäytteitä metallo-organisella kaasufaasiepitaksialla. Työn näytteet karakterisoitiin fotoluminesenssi- ja atomivoimamikroskopiamittausmenetelmillä. InAs-saarekkeiden koko ja tiheys optimoitiin ensiksi sopivaksi SOA-rakennetta varten valmistamalla itseorganisoituvia InAs-saarekkeita suoraan InP päälle. Näitä tuloksia käytettiin optimoidun InGaAsP-kerroksen sisältävän rakenteen valmistuksessa. Atomivoimamikroskopiamittaus paljasti, että optimoidun rakenteen InAs-saarekkeet olivat keskimäärin 10 nm korkeita ja 30 nm leveitä. Kvanttipisteiden luminesenssipiikin maksimi havaittiin 1.56 μm aallonpituudella 10 K lämpötilassa.

Avainsanat: Indiumarsenidi, indiumfosfidi, indiumgalliumarsenidifosfidi, kvanttipiste, optinen puolijohdevahvistin, metallo-organinen kaasufaasiepitaksia.

Preface

This thesis has been carried out in Optoelectronics group at the Department of Micro and Nanosciences at Aalto University. I would like to thank Professor Markku Sopanen for providing me with the oppurtunity to work in the Optoelectronics group while similarly carring out this thesis. I also would like to thank him for everything I have learned during numerous interesting discussions with him related to this thesis. Furthermore, I would like to thank my thesis instructor Docent Teppo Hakkarainen for all the help and guidance he has given me during this work. In addition to this, I would like to thank my other thesis instructor Dr. Abuduwayiti Aierken for teaching me the secrects behind the MOVPE apparatus, and also always providing help when I have needed it.

I want to thank M.Sc Päivi Mattila and Dr. Nagarajan Subramaniyam for all the support and help they have given me during this thesis work. I own great compliments to them. I also want to thank the whole personnel of the department of the Micro and Nanosciences for the inspiring and nice athmosphere that have encouraged me to come to work excited day after day.

Finally, I want to thank my parents and my brother for all the support they have given me. Without you this thesis would never have been possible.

Otaniemi, 30.3.2010

Henri Jussila

Contents

List of acronyms

AFM	atomic force microscopy
AlGaN	aluminium gallium nitride
DOS	density of state
EDFA	erbium doped fiber amplifier
FCC	face centered cubic
FM	Frank-van der Merve growth mode
FWHM	full-width-at-half-maximum
GaAs	gallium arsenide
GaN	gallium nitride
InAs	indium arsenide
InGaAsP	indium gallium arsenide phosphide
InP	indium phosphide
LT-PL	low-temperature photoluminescence
MFC	mass flow controller
ML	monolayer
MOVPE	metalorganic vapor phase epitaxy
PL	photoluminescense
QD	quantum dot
QW	quantum well
RT-PL	room-temperature photoluminescence
SK	Stranski-Krastanow growth mode
SOA	semiconductor optical amplifier
TBAs	tertiarybutylarsine
TBP	tertiarybutylphosphine
TEM	transmission electron microscopy
TMGa	trimethylgallium
TMIn	trimethylindium
VW	Volmer-Weber growth mode
WL	wetting layer
XRD	X-ray diffraction

1 Introduction

In recent years, continuous improvements in optical data transfer systems have enabled the modern information society. At present, vast amount of information coded in optical signals propagates all around the world inside optical fibers. Optical signals in long-haul networks have a wavelength of 1.55 μm which corresponds to the absorption minimum of light in silica fibers. However, the intensity of these signals still considerably decays without amplification. Therefore, efficient optical amplifiers are required. Previous research has provided many suitable amplifier solutions for operation at telecommunication wavelengths [1]. For instance, erbium doped fiber amplifiers (EDFAs) are able to amplify optical signals inside the fibers [2]. Semiconductor optical amplifiers (SOA) are used in applications that amplify the optical signals outside the optical fibers [3].

Previously, telecommunication wavelength region SOAs have been fabricated from indium gallium arsenide (phosphide)/indium phosphide (InGaAs(P)/InP)-based bulk and quantum well (QW) materials [4, 5]. In recent years, indium arsenide (InAs) quantum dot (QD) and quantum dash structures grown on InP substrates have been examined and fabricated as a new solution for telecommunication wavelength region components [6, 7]. In order to realize the full potential of these components, a significant amount of effort has been addressed to characterizing the properties of InAs/InP QDs [8-14]. It has been shown that InAs QD layer can provide higher light emission efficiency than conventional InGaAsP/InP QW layer [11]. Therefore, InAs QDs on InP substrates could potentially provide a material that enables telecommunication wavelength SOAs to operate more efficiently. Although these materials are promising, many problems still remain to be solved for developing high-quality materials for commercial applications.

In this Master′s thesis, InAs QDs have been grown by metalorganic vapor-phase epitaxy (MOVPE) technique on InP substrates, and their properties have been investigated. Photoluminescence (PL), atomic force microscopy (AFM), and X-ray diffraction (XRD) were used in the characterization of the optical and the structural properties of the samples, respectively. InAs island size and the areal density was first optimized for SOAs by growing self-assembled InAs islands directly on InP. These results were used to finalize the structure containing also InGaAsP waveguide layer. AFM results show that InAs islands, which eventually form the QDs, were grown quite homogenously on InGaAsP with an average height of 10 nm and an average base diameter of 30 nm. The low temperature PL peak of the InAs/InGaAsP/InP QDs was tuned to the wavelength of 1.56 μm.

This thesis is organized as follows. Chapter 2 reviews the basic theory related to InAs/InGaAsP/InP QD SOAs. Chapter 3 explains the MOVPE fabrication method and the fabrication of InAs/InGaAsP/InP QD structures. Chapter 4 reviews AFM, PL and XRD experimental methods which are used in the characterization of the samples. Chapter 5 presents the obtained results. Finally, chapter 6 concludes this thesis.

2 Theoretical

This chapter describes the background of the theory related to the InAs QD SOAs. The chapter is organized in the following way. Section 2.1 explains the fundamentals of solid state physics of semiconductors. Section 2.2 discusses the quantum mechanical effects occurring inside quantum structures. Section 2.3 reviews the basic theory of semiconductor optical amplifiers. In addition to this, the structure of an InAs QD SOA is presented in section 2.3.

2.1 Solid state physics

2.1.1 Crystal structure

Atoms in solid state materials are located at energetically most favorable sites. The locations depend on the chracteristics of the atoms, such as their size and their electric structure. Generally, the ordering of the atoms can be monocrystalline, polycrystalline or amorphous. III-V compound semiconductor materials made by epitaxy tend to crystallize into a monocrystalline structure. Therefore, the theory below relate to monocrystalline solid state materials, *i.e.*, crystals.

When materials crystallize the atoms are arranged into a crystal lattice. The crystal lattice represents a set of points in space which form a periodic structure. The smallest repetitive structure in any crystal lattice is called the primitive unit cell. The whole crystal can be formed by repeating primitive unit cells. Primitive vectors are linearly independent and connect the lattice points of crystal lattice. Primitive vectors can be chosen by numerous ways and, therefore, primitive vectors are not unique. Primitive vectors have a useful property that all the lattice points $\mathbf{R}$ can be derived from one lattice point $\mathbf{R}'$ when some linear combination of primitive vectors is added to it. In other words,

$$\mathbf{R} = \mathbf{R}' + m_1\mathbf{a_1} + m_2\mathbf{a_2} + m_3\mathbf{a_3},$$

where m_1, m_2 and m_3 are integers, and $\mathbf{a_1}, \mathbf{a_2}$ and $\mathbf{a_3}$ are the primitive vectors. As a result of this, the whole crystal can be formed by choosing all combinations of the integers m_1, m_2 and m_3.

III-V compound semiconductor materials fabricated for this thesis crystallize into the zinc-blende crystal lattice. To illustrate this type of crystal lattice, a conventional unit cell of a face centered cubic (FCC) lattice is shown in figure 1. Atoms in FCC lattice are located at every corner and at the center of every face of a cube. The zinc-blende lattice is composed of two separate FCC sublattices one of which is comprised of group-III atoms and the other of group-V atoms. The dimensions of the two FCC-lattices are equal but the origin of the other lattice is displaced from the other by a vector $(\frac{a}{4}, \frac{a}{4}, \frac{a}{4})$ along the body diagonal. Figure 2 illustrates the conventional unit cell of a zinc-blende crystal lattice, and table 1 presents the

basic crystalline properties of different binary III-V compound semiconductors. The lattice constant of a zinc-blende crystal is defined as the length of the conventional unit cell.

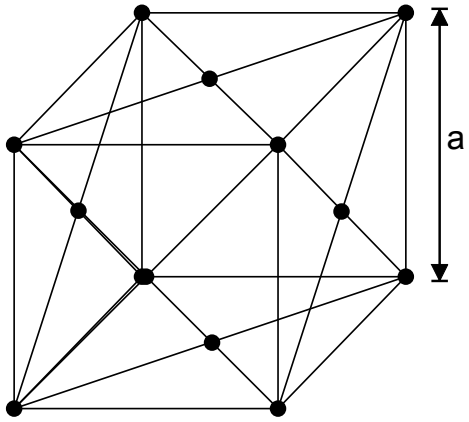

Figure 1: Conventional unit cell of FCC lattice. The primitive vectors could be chosen, *e.g.*, as the vectors which connect one corner to the center of the three nearest faces.

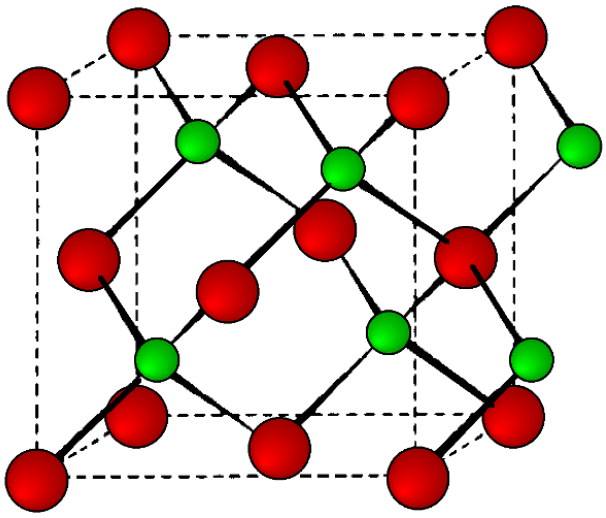

Figure 2: Conventional unit cell of the zinc-blende lattice [15].

2.1.2 Energy band structure

The energy band structure is an extremely useful concept, and is used to explain the electronic structure of the material. Energy band structure is derived from quantum

	lattice constant (å)	crystal structure
InAs	6.06	zinc-blende
InP	5.87	zinc-blende
GaAs	5.65	zinc-blende
GaP	5.45	zinc-blende

Table 1: Crystalline properties of binary III-V compound semiconductors.

mechanics. The foundation of quantum mechanics is the Schrödinger equation, represented in time independent form as

$$(-\frac{\hbar^2}{2m}\nabla^2 + V(\mathbf{r}))\psi(\mathbf{r}) = E\psi(\mathbf{r}), \tag{1}$$

where ∇ is the gradient, $\hbar$ is the Planck's constant, and m is the mass of the particle. $V(\mathbf{r})$ denotes the potential energy experienced by the particle. Typically in solids, potential energy is comprised of interactions between the particle and all the atoms in solids. Therefore, Schrödinger equation is very difficult to solve. Still, many numerical and approximative techniques have been applied, and consequently the energy band structure of solids is quite well-known.

In semiconductor crystals, the potential energy is always periodic, *i.e.*,

$$V(\mathbf{r}) = V(\mathbf{r} + \mathbf{a}),$$

where $\mathbf{a}$ is the primitive vector of the material. Bloch's theorem explaines the nature of the wave functions and energy states when the potential energy is periodic. As a result of the theorem, periodicity of the atoms makes the energy states of crystals periodic in E-$\mathbf{k}$ space, where $\mathbf{k}$ is the electron wavevector. In addition, the semiconductor crystals have some energies which are forbidden for every $\mathbf{k}$-vector.

The relation between the electron wavevector $\mathbf{k}$ and the energy E is called the dispersion relation. Allowed energy states in E-$\mathbf{k}$ space form continous energy bands. The two most important energy bands in semiconductors are the valence band and the conduction band. The valence band is defined as the highest occupied energy band, and the conduction band as the lowest empty energy band at the temperature of 0 K. Band gap of the material is defined as the energy difference between the conduction band minimum and the valence band maximum. Table 2 presents the band gaps of different III-V compound semiconductors.

All optical processes occurring in different materials follow the conservation laws of energy and momentum, and can be described with E-$\mathbf{k}$ diagrams. For optoelectronic devices in general, the emission and absorption of light are the most important optical processes. As a result of these processes, the electrons inside materials are either excited to higher energy states or relaxed to lower energy states. Important material characteristics for optoelectronic devices is whether the band gap is direct or indirect. This is illustrated schematically in figure 3. In direct band gap materials,

	band gap in eV	corresponding emission wavelength (nm)
InAs	0.354	3506
InP	1.344	924
GaAs	1.424	871
GaP	2.26	549

Table 2: Band gap and corresponding emission wavelength of various binary III-V compound semiconductors.

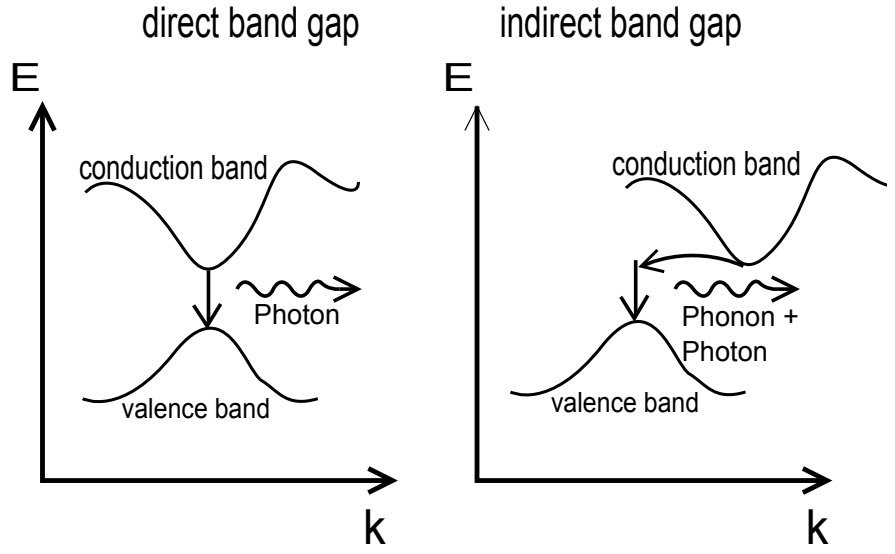

Figure 3: Energy band structures and photon generation in direct and indirect band gap semiconductors. The generation of a photon in indirect band gap material requires a change of momentum (*i.e.*, the wavevector $\mathbf{k}$).

the conduction band minimum is located at the same $\mathbf{k}$-vector value as the valence band maximum. The operation of optoelectronic devices that emit or amplify light is based on the phenomenon of either luminescence or stimulated emission. In these phenomena, an electron is relaxed from the conduction band to the valence band, thus generating a photon whose energy equals to the difference of these energy states. In indirect band gap materials, these phenomena are inefficient because the energy transition between the conduction band and the valence band requires a change in momentum which usually occurs via an interaction with a phonon. Therefore, direct band gap materials are typically used in optoelectronic devices.

2.1.3 III-V compound semiconductors

III-V compound semiconductors are composed of group III and group V atoms, and are mainly used in optoelectronic applications because of their bandstructure characteristics. InP, InAs, gallium arsenide (GaAs), and gallium nitride (GaN) exemplify

binary alloys (two elements). Ternary alloys (*e.g.*, InGaAs, aluminium gallium arsenide (AlGaN)) are composed of three different elements, and quarternary alloys (*e.g.*, InGaAsP, InAlGaAs) of four. III-V compound semiconductors provide the possibility to engineer the band gap and the lattice constant by changing the composition of the different elements. Figure 4 shows the relation between the crystal structure and the energy band gap of different III-V compound semiconductors.

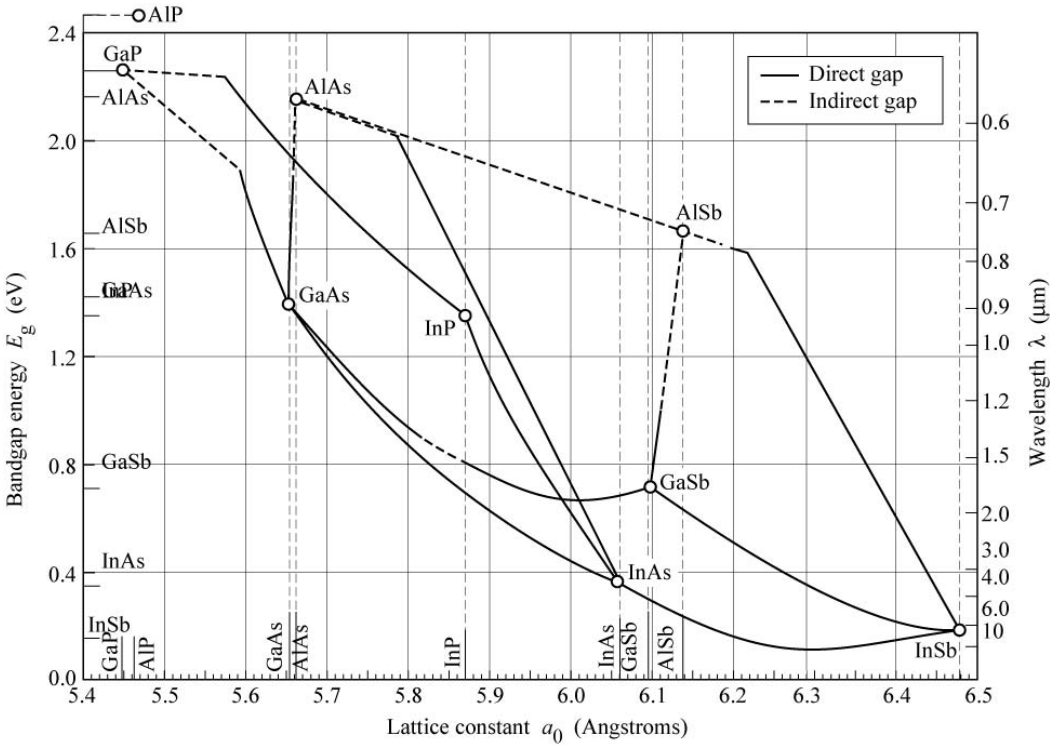

Figure 4: Band gap and the lattice constant of different III-V compound semiconductor materials [16]. The lines drawn in the image describe the lattice constant and the band gap of different ternary alloys. For instance, the band gap and the lattice constant of $In_{(1-x)}Ga_xAs$ is located on the line which is drawn between the binary compounds GaAs and InAs.

2.2 Quantum structures

Quantum structures confine the charge carriers in one, two or three dimensions to such a small size that quantum mechanical effects are observed. The structure which confines the charge carriers in one dimension is called a QW. QWs can be fabricated by growing a layer of a small band gap material sandwiched between a large band gap material. Electrons in the small band gap material experience a potential energy well when moving along the growth direction. The structure which confines the charge carriers in two spatial dimensions is called quantum wire. QDs confine the charge carriers in all three spatial dimensions. Fabrication of QDs can be performed by different methods, all of which result in a structure where a small

band gap material is located inside a large band gap material. Figure 5 illustrates the bulk, QW, and QD structures.

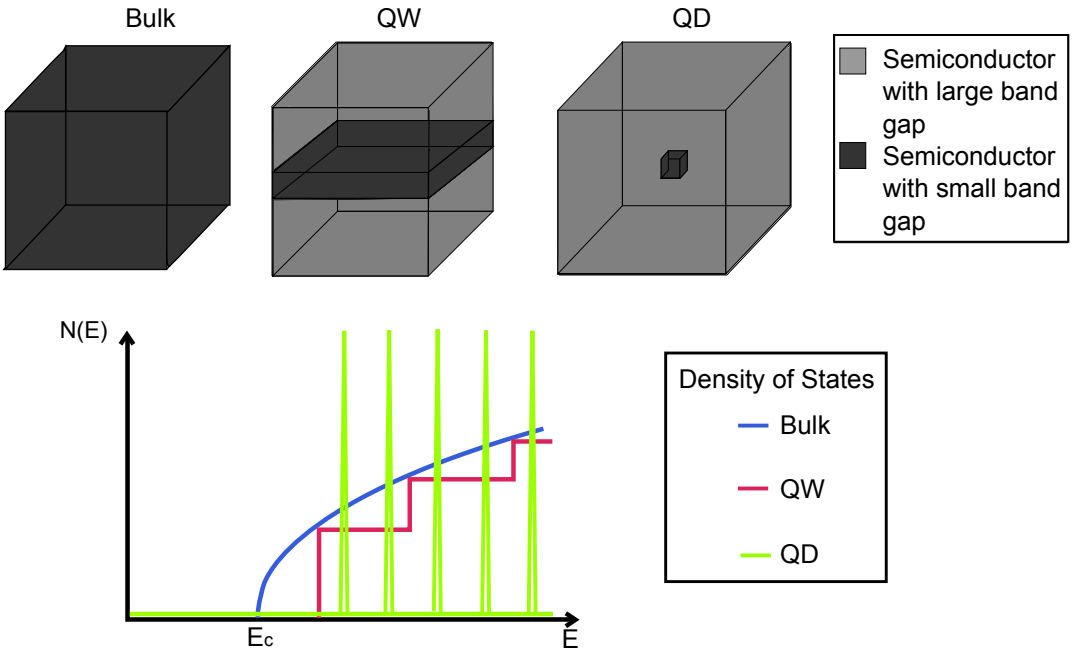

Figure 5: The ideal geometrical structure and the DOS function of bulk, QW, and a single QD. E_c describes the energy corresponding to the conduction band edge.

2.2.1 Semiconductor quantum wells and quantum dots

In recent decades, quantum structures have been intensively examined because of their interesting properties that are presented next. Quantum structures provide the possibility to engineer the energy band structure of the material. The dispersion relation of the conduction band is presented for bulk semiconductors and different quantum structures. The similar results are also valid for the valence band with the only difference then occurring in the effective mass of the electron, which is replaced by the effective mass of the hole in the valence band.

The dispersion relation of the bulk material is assumed to be parabolic near the band edge (*i.e.*, near the Γ-point, $\mathbf{k} = \mathbf{0}$) [17]. Hence,

$$E_{bulk}(\mathbf{k}) = E_g + \frac{\hbar^2}{2m_e}\mathbf{k}^2, \tag{2}$$

where the E_g is the band gap of bulk material, and m_e the effective mass of electron. The zero of the energy is set at the valence band maximum.

The dispersion relation of a QW with an infinitely high barriers gives the following energy states:

$$E_{QW}(\mathbf{k}) = E_g + \frac{\pi^2\hbar^2 n^2}{2m_e L^2} + \frac{\hbar^2}{2m_e}\mathbf{k}_{\|}^2, \tag{3}$$

where $\mathbf{k}_{||}$ is the wavevector component in the quantum well plane, L the width of the quantum well, and n any integer. The solution is valid only near the energy band edge.[17] The conduction band minimum (n=1) for the QW is located at a different energy than for the bulk material, and the width of the quantum well affects the allowed energy states. Therefore, the energy band position of the QW structure can be engineered by varying the thickness of the QW.

For a spherical QD structure with infinitely high barriers the allowed energies are

$$E_{QD}(\mathbf{k}) = E_g + \frac{\hbar^2}{2m_e}(\frac{\kappa_{n,l}}{R})^2, \tag{4}$$

where $\kappa_{n,l}$ is the n^{th} zero of l^{th} Bessel function and R the radius of the quantum dot [18]. The radius of the QD affects the energy states, so again the energy bands can be engineered by varying the size of the quantum structure. In addition to this, the energy states of QDs are completely discrete.

The height of the potential barrier was set to infinite to obtain previous results. In real semiconductor QW and QD systems this infinite potential well approximation is not true; and in fact, the height of the potential well also affects the allowed energy states of real quantum structures. However, the results obtained using this approximation provide insight into the nature of the energy states and are not far from the ones obtained by the more advanced numerical techniques.

Quantum structures provide attractive means to engineer the energy band structure of the material. In addition to this, quantum structures possess one extra advantage which is their density of state (DOS) function. DOS function explains how electrons can occupy the energy states of the structure. For instance, if the DOS function has a value of zero for some energy, then no electron can occupy that energy state. Figure 5 illustrates the DOS functions of different quantum structures. The DOS function in bulk materials is propotional to the square root of the energy. In quantum structures, the charge carriers are more strictly confined to specific energy states. QWs have a step-function-like DOS function and QDs have a delta-function-like DOS function. The delta-function-like DOS function is the main reason why QDs have been of great interest in recent years. This type of DOS function ensures that the charge carriers are strictly confined to the energy states described in the equation 4. Therefore, QD structures enable the fabricatation of components that, in principle, operate extremely efficiently.

2.2.2 Real quantum dot systems

The fabrication of real QD systems is a difficult process, and results in nonidealities compared to the theory presented in section 2.2.1. Semiconductor QDs are

fabricated, *e.g.*, by the following techniques. First techniques used for the fabrication of QDs and quantum wires included lithography and etching steps [19, 20, 21]. The etching step resulted in degradation of the crystal structure of the material. Later, in-situ growth of coherent (*i.e.* dislocation free) QDs was invented. This self-assembled technique is based on the Stranski-Krastanow growth mode of thin films [22]. The term self-assembly refers to the behaviour of the adsorbed atoms to form islands without any external interactions. In this technique, the self-assembly emerges due to the crystal lattice mismatch between the two different materials; and as a result of this, QDs are then fabricated from these islands. This growth mode is explained in more detail in section 3.2.2.

As explained in the previous section, QDs emit luminescence at discrete energies because of their DOS function. However, the luminescence spectrum in real QD systems has not fully realized this promise and QD structures can have relatively broad luminescence spectra compared to QWs. This broadening originates from the fabrication processes of the QDs. For instance, the broadening in self-assembled QDs comes from the size distribution of the islands fabricated by the coherent Stranski-Krastanow growth mode. In practise, the growth conditions in the self-assembled technique are optimized so that the fabricated QDs are as homogenous as possible. Still, QDs with different sizes always exist in real QD structures. As seen from equation 4, the size of the QD affects the energy states significantly.

In addition to this, the luminescence intensity of the QD energy states has usually been lower compared to QW structures, for example. First, this was attributed to the reduced material quality resulting in the fabrication process of the QDs. However, it has later been suggested that this poor luminescence can result from the relaxation processes of the charge carriers [23, 24]. This phenomenon is called the phonon bottleneck of charge carriers. In order to observe luminescence from QDs, charge carriers first have to relax close to the QD energy state minima. In general, the charge carriers can relax in the energy band minima with many relaxation mechanisms. The most usual mechanisms are via Coulomb interaction and Auger process, and the relaxation induced by an interaction with a phonon. To explain the inefficiency of the QD luminescence it has been suggested that the relaxation of charge carriers is a significantly slower process in QDs than in QW and bulk materials due to the more discrete energy states of QDs. Scattering occurs mainly via Auger and Coulombic processes. The relaxation processes via the phonons are more improbable in QDs since only few phonons have suitable energies for interaction. [25]

2.3 Semiconductor optical amplifier

SOAs are semiconductor components which amplify optical signals directly without any optical-to-electrical conversions outside optical fibers. SOAs are comprised of the waveguide structure and the gain media. The waveguide structure maintains the optical signal inside the component, and the gain media inside the waveguide amplifies the optical signals. A SOA component usually has the following size: a

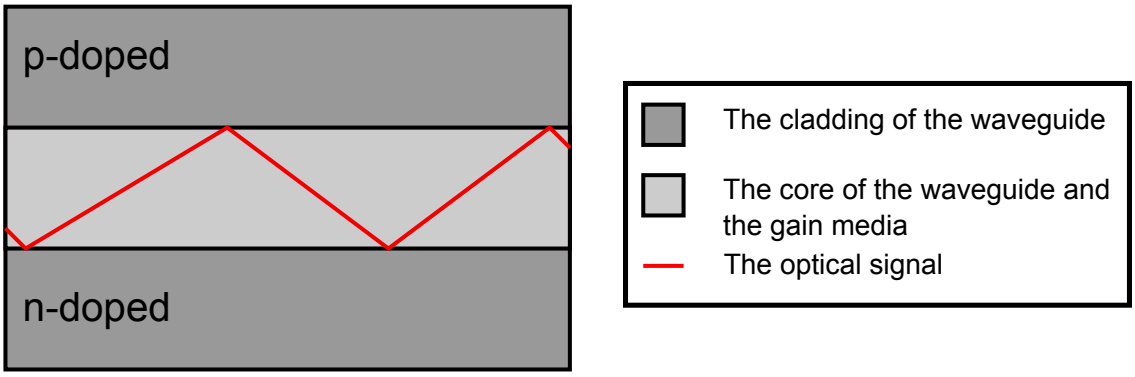

Figure 6: The crossection of SOA.

length between 0.5 and 2 mm, and a transverse distance between 1 and 2 μm [26]. In addition to this, the waveguide is coated by an anti-reflection coating at the both ends of the waveguide to prevent optical signals from reflecting back to the waveguide. The structure of the SOA is similar to the structure of a laser diode. However, in the laser diodes the anti-reflection coatings are replaced by end-mirrors. Figure 6 illustrates the structure of the SOA.

The optical processes occurring inside the gain medium can be represented in a simplified form by energy band diagram with only the conduction and the valence band energy levels, E_c and E_v. The amplification is based on stimulated emission which is the process depicted in figure 7a. In stimulated emission, a photon propagates near an electron which occupies an energy state in the conduction band, E_c, thus causing the radiative relaxation of the electron. The energy and the phase of this new photon equal the energy and the phase of the incoming photon. As a result, the optical signal is thereby amplified. Other processes in figure 7 are called stimulated absorption and spontaneous emission. When these processes occur inside the waveguide they cause disturbance to the signal. In stimulated absorption, a photon is absorbed, thus resulting in loss of the intensity of the optical signal. Electrons in the conduction band can also recombine spontaneously to valence band generating photons. Spontaneous emission causes noise because the emitted photons have random phase distribution.

Population inversion is a statistical situation describing a certain state of the charge carriers in the gain media of the SOA. Population inversion is created if more electrons occupy the conduction band energy state, E_c, than the valence band energy state, E_v. Population inversion is extremely important for the operation of the SOA because without population inversion the absorption would be the most dominant optical process inside the waveguide. In SOAs, the population inversion is created electrically inside the waveguide. The waveguide is located inside the depletion region of a pn-junction; and therefore, charge carriers drift to the waveguide area when the voltage is applied over the junction.

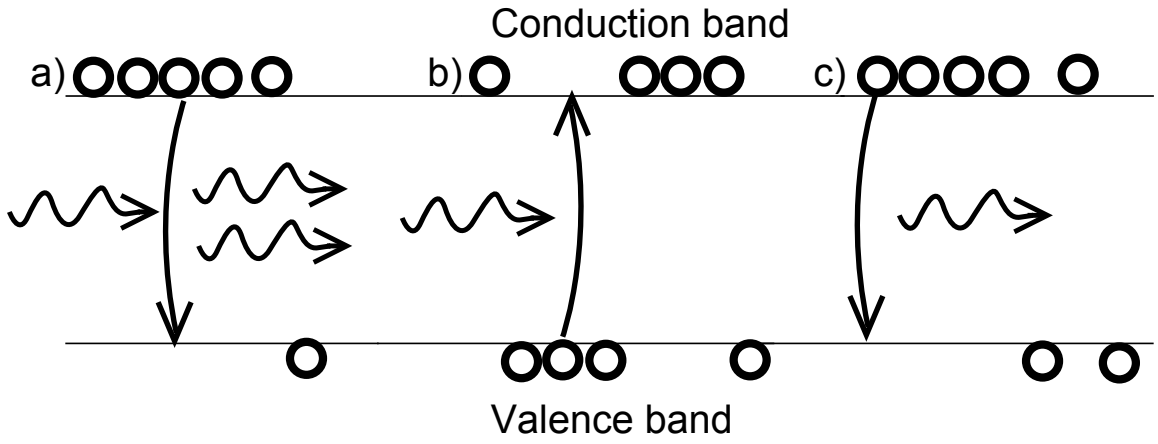

Figure 7: Different optical processes occurring in the active media of the SOA: (a) stimulated emission (b) stimulated absorption and (c) spontanous emission.

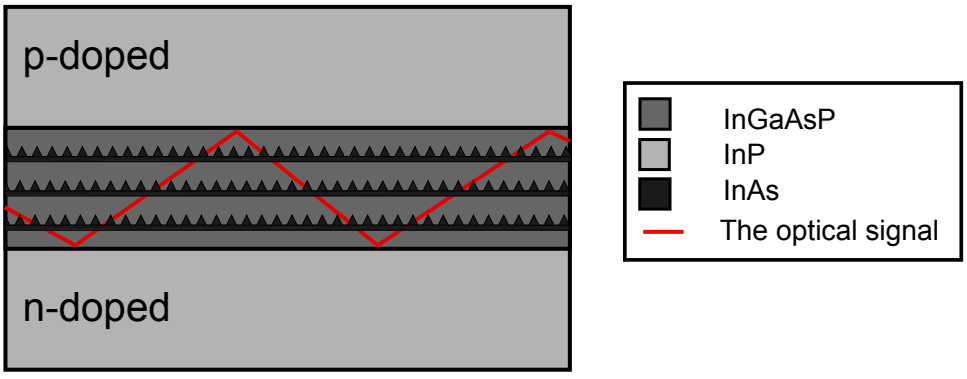

Figure 8: Crossection of an InAs QD SOA with three layers of InAs QDs.

SOAs compete with EDFAs in the field of amplification of optical signals. Usually the choice between a SOA and an EDFA depends on the application where the component is used. Advantages of the SOAs are a small size, and the price of a single component. In addition, population inversion is created electrically which can be beneficial in some applications; and furthermore, SOAs are integrable with semiconductor laser diodes and modulators. However, in some cases the performance of SOAs is not comparable to that of EDFAs. The noise is much higher in SOAs because of the short upper energy state lifetime of charge carriers. This can also cause crosstalk between channels in wavelength division multiplexing (WDM) applications, in which many wavelength channels are amplified simultaneously. In addition to this, the output power is smaller in SOAs, and the amplification is polarization sensitive which can be harmful in some situations. [26]

2.3.1 Indium arsenide quantum dot semiconductor optical amplifier

The structure of an InAs/InGaAsP/InP QD SOA is introduced in this section and compared to the earlier SOA devices. Figure 8 presents a schematic illustration of this device. GaAs/AlGaAs material combination was used to fabricate the first SOAs. These devices amplified signals at near-infrared wavelengths (ca. 800 nm). Later, most of the SOA research has been focused on InGaAs(P)/InP materials. QW and bulk components fabricated from these material combinations are used to amplify optical signals which propagate at telecommunication wavelengths of 1.3 μm and 1.5 μm. [5]

InAs/InGaAsP/InP QD SOA utilizes the delta-function-like DOS function of a single QD, and aims to amplify optical signals propagating at the telecommunication wavelengths. In contrast to the bulk and QW SOAs, this type of SOA could potentially operate more efficiently in WDM applications. In bulk and QW SOAs, the amplification of one channel reduces the gain of another channel. This phenomenom is not encountered in QD SOAs in which QDs with specific size can only amplify signals propagating at one wavelength. Therefore, the broad size distribution of the QDs resulting from the Stranski-Krastanow growth mode is actually beneficial for the operation of the component. The broad size distribution ensures that every wavelength channel has QDs suitable for the amplification of that channel.

3 Metalorganic vapor phase epitaxy

MOVPE is a standard growth method used in the fabrication of III-V compound semiconductors. This chapter explains the theory related to this fabrication method. The processes occurring inside the MOVPE apparatus are extremely complex. Therefore, the aim of this chapter is not to perform a complete discussion about the fundamentals of this method as they are understood at the moment. On the contrary, the aim of this chapter is more to explain the phenomena occurring inside the MOVPE apparatus, and how they are utilized in order to grow samples with good quality. The chapter is organized in the following way. Section 3.1 presents the source materials used in the growth of the InAs/InP QD samples. In addition, the kinetics of their pyrolysis reactions is discussed in this section. Section 3.2 explains the surface processes and epitaxial growth modes of thin films. Section 3.3 discusses the mass-transport controlled growth occurring in an actual MOVPE reactor. Section 3.4 presents the setup of the MOVPE apparatus, and section 3.5 discusses the fabrication of the InP-based compound semiconductors.

3.1 Source materials and pyrolysis

MOVPE uses organometals as source materials. Organometals are carbon compounds which are comprised of carbon, hydrogen, and group III and group V atoms. Organometals are toxic materials (particularly tertiarbutylphosphine (TBP) and tertiarbutylarsine (TBAs)). At room temperature, organometals in general are in liquid or in solid state. The fabrication of InAs QDs was performed using the following sourcematerials: trimethylindium (TMIn), trimethylgallium (TMGa), TBAs, and TBP. Table 3 presents some properties of these materials.

Source material	chemical compound	molar mass (g/mol)	melting point (°C)	vapor pressure (torr)
TMIn	$(CH_3)_3In$	159.85	88	1.71 (at 20°C)
TMGa	$(CH_3)_3Ga$	114.82	-15.8	36.8 (at -10°C)
TBP	$C_4H_9PH_2$	90.10	4	217 (at 20°C)
TBAs	$C_4H_9AsH_2$	134.05	-1	81.4 (at 10°C)

Table 3: Basic properties of organometallic source materials [29].

Organometals start to decompose when they are heated up inside the MOVPE reactor. This reaction is called the pyrolysis. The pyrolysis of every organometal is an extremely complex phenomenom. In addition to this, each organometal experiences pyrolysis reactions during the growth at the same time, thus resulting in bimolecular reactions between the different source materials. [27] Furthermore; flow velocity, pressure, temperature, and the shape of the MOVPE reactor all have an effect on the pyrolysis reactions. Therefore, the kinetics of the pyrolysis reactions can not be completely modelled. Despite that, it is experimentally known for most source materials that pyrolysis occurs via certain reactions at certain temperatures. This

is sufficient for succesful growth of good-quality III-V compound semiconductors. To exemplify the complexity of the pyrolysis reactions more, the reaction chain of the pyrolysis of TMIn is presented next.

The pyrolysis of TMIn is complete at temperatures of over 350° [27]. The pyrolysis reactions of TMIn are suggested to occur via the following reactions: [28]

$$(CH_3)_3In \leftrightarrow (CH_3)_2In + CH_3, \tag{5}$$
$$(CH_3)_2In \leftrightarrow (CH_3)In + CH_3, \tag{6}$$
$$(CH_3)In \leftrightarrow In + CH_3, \tag{7}$$
$$n(CH_3)In \leftrightarrow (In(CH_3))_n. \tag{8}$$

Complete utilization of TMIn requires temperatures higher than 480°C. This is due to the fact that reaction 7 is unlikely at temperatures less than that. At lower temperatures, the reaction is replaced by reaction 8, and the polymeric compound $(In(CH_3))_n$ is formed. Reactions 5 and 6 are homogenous, which means that pyrolysis reactions occur in the gas phase, whereas reaction 7 is heterogenous. This means that the reaction occurs both between the gas phase and the solid phase and in the gas phase.

The reaction chains of the pyrolysis reactions of TMGa, TBAs, and TBP are known in a similar way. It should be noted that the completeness of the pyrolysis requires different temperatures for different source materials. The pyrolysis of TMGa and TBP are complete at temperatures of higher than 450°C, and higher than 550°C, respectively. The complete pyrolysis of TBAs requires temperatures of higher than 500°C. [27] In addition to this, it should be mentioned that the simultaneously occuring pyrolysis reactions of different source materials can increase, decrease or not affect the reaction rates and the pyrolysis temperatures of other precursors. For instance, the presence of TBAs increases the reaction rate of the pyrolysis of TMGa, and the pyrolysis of TBP requires higher temperature when TMGa is inside the reactor. [29]

3.2 Surface processes and epitaxial growth

MOVPE is a chemical fabrication method for inorganic crystals. A thermodynamic nonequilibrium state, which is created intentionally inside the MOVPE reactor during growth, drives the pyrolyzed source material molecules eventually to the surface of the substrate crystal.

3.2.1 Surface processes and heteroepitaxy

Growth of III-V compound semiconductors begins from the pyrolysis reactions explained in section 3.1. These pyrolysis reactions occur inside the MOVPE reactor, thus resulting in the appearence of the free group-III and group-V atoms in the

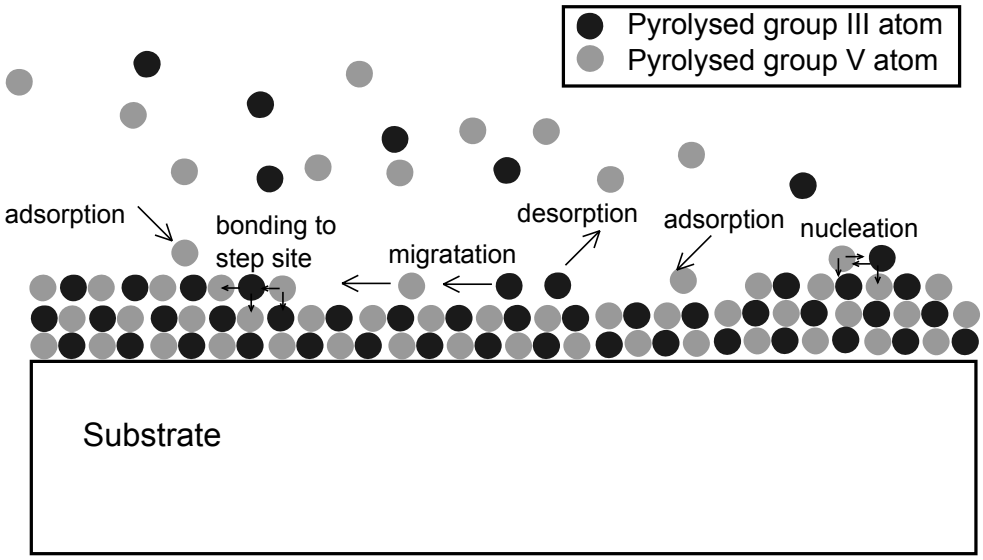

Figure 9: Principal surface processes occurring during growth of a binary III-V compound semiconductor.

gas phase. Then, these atoms diffuse near to the surface of the substrate. After that, these atoms can be adsorbed to the surface. In addition to this, atoms that are already located on the surface can be desorbed. These adsorption, desorption and diffusion processes occur simoultaneously and originate from the attempt of the system to obtain thermodynamic equilibrium. A key to succesful growth is to create such conditions inside the reactor that atoms preferably are adsorbed to the surface of the substrate. Figure 9 presents the most important processes experienced by the atoms near and on the surface of the substrate. These processes include migration of atoms, nucleation, and bonding to step or kink sites. Surface processes are driven by the attempt of the thin film to minimize its total energy making some reactions more probable than the others. Temperature inside the reactor and the material combinations greatly affect the probabilities of different processes.

Growth of III-V compound semiconductor materials occurs epitaxially inside the MOVPE reactor. The term epitaxy refers to a growth mode where the growing atomic layers copy the crystal structure of the substrate. In heteroepitaxial growth, one material is grown epitaxially on top of a different material. Therefore, heteroepitaxial growth can add stress to the crystal because atoms have to accomodate to the crystal lattice underneath them. Figure 10 illustrates the lattice structure behaviour in heteroepitaxy.

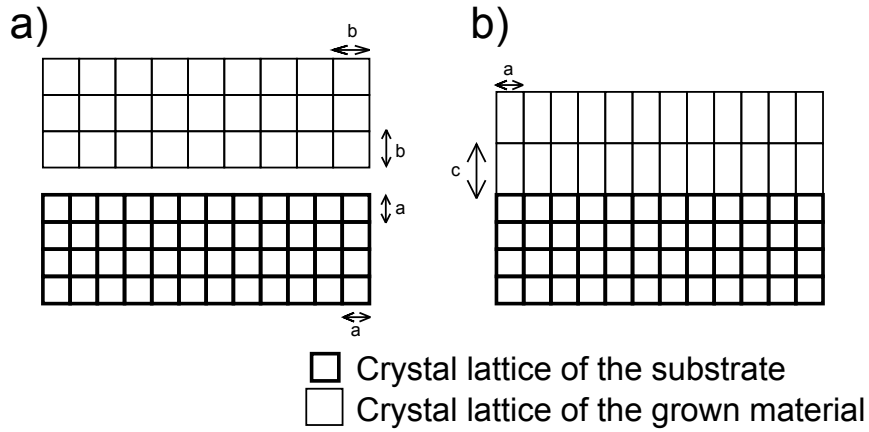

Figure 10: Simplified crystal lattice of (a) two different materials with lattice constants a and b, and (b) the same materials in a heteroepitaxially grown structure. The crystal lattice of the grown material adapts to that of the substrate.

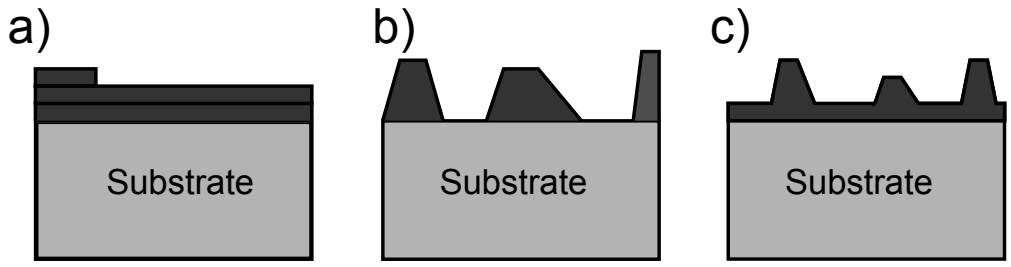

Figure 11: Different growth modes of thin films: (a) FM growth mode, (b) VW growth mode and (c) SK growth mode. The darker area reflects the grown material and the lighter area the substrate, respectively. The crystal structure of the substrate is copied in the upper layers.

Figure 11 shows the different possible growth modes of thin films. These growth modes are a result of the thin film attempting to minimize its total energy. Figure 11a shows the Frank-Van der Merwe (FM) growth mode where the growth occurs two-dimensionally one layer at the time. Figure 11b illustrates the Volmer-Weber (VW) growth mode. In this growth mode, adsorbed atoms form clusters and three-dimensional islands but do not wet the surface. Figure 11c shows the Stranski-Krastanow growth mode where the first grown atomic layers remain smooth two-dimensional layers; and then, islands start to form. The two-dimensional layer is called the wetting layer (WL). The Stranski-Krastanow growth mode is explained in more detail in the next section.

3.2.2 Stranski-Krastanow growth mode

At present, growth of QDs from III-V compound semiconductor materials is mostly performed by exploiting the Stranski-Krastanow (SK) growth mode. The ignition for this research happened in the beginning of 1990's when it was observed that the self-assembled islands grown by SK growth mode were coherent (*i.e.* dislocation free). The SK growth mode is today used in the fabrication of QDs from various material combinations, such as $In_{(1-x)}Ga_xAs/GaAs$, GaSb/GaAs, and InAs/GaAs [35]. Also, the InAs QDs examined in this thesis were grown by self-assembly of InAs on InP. As described, SK growth mode can be characterized by the transition from 2D to 3D growth mode. To explain this transition a brief discussion relating to the total energy of thin films is required.

In general, the growth mode is determined by the attempt of the thin film to minimize its total energy. The most important components of this total energy are surface energy, strain energy, interface energy, and dislocation energy. Two-dimensional FM growth mode occurs when the surface energy of the thin film is lower than the surface energy of the substrate. In addition, the strain energy of the thin film is small. Usually, this situation is encountered when growing amorphous, polycristalline or near-perfectly lattice-matched epitaxial thin films. The three-dimensional VW growth mode occurs if the film has high surface energy compared to the surface energy of the substrate. Then, it is energetically more favorable for the thin film to form clusters. In the SK growth mode, the surface energy of a smooth film is small compared to the substrate. Therefore, the first adsorbed atoms form a smooth two-dimensional surface. However, the strain energy of the surface begins to increase when the thickness of the film increases. After certain critical thickness has been reached, the strain energy of the film is so large that it is energetically more favorable to grow by forming clusters. [30]

3.3 Mass-transport controlled growth

As explained in the sections 3.1-3.2, growth of III-V compound semiconductors begins from the pyrolysis reactions. Then, the thermodynamic nonequilibrium state forces the atoms to diffuse and adsorb onto the substrate. However, growth occurring in the actual apparatus is not limited by the kinetics of the pyrolysis reactions. Moreover, the reaction rate at the surface of the sample is high compared to the diffusion of the source atoms. Therefore, thermodynamic equilibrium is never reached in MOVPE growth. The growth is mass-transport controlled; and thereby, diffusion limited.

The growth rate of the III-V compound semiconductors depends on the flow rates of different source materials. During growth, the temperature inside the reactor is between 400°C and 700°C, thus enabling the pyrolysis reactions of the source materials. However, this temperature also allows atoms to desorb from the substrate. The group V atoms are more easily desorbed from the substrate than group III atoms [29]. Therefore, group V source materials are constantly supplied at a higher rate

in the MOVPE reactor to protect the surface of the sample.

The flow rate of group III atoms is lower than the flow rate of group V atoms. Therefore, the group III atoms define the growth rate of the material, r_g, which is propotional to

$$r_g \propto p^*_{III}\sqrt{\frac{F_{total}}{P}}, \tag{9}$$

where F_{total} is the total flow to the reactor, P the pressure inside the reactor, and p^*_{III} the partial pressure of the group three atoms. [29] The partial pressure of any species i, p^*_i, is given as:

$$p^*_i = P\frac{p_{vapor,i}}{p_{source,i}}\frac{F_i}{F_{total}}, \tag{10}$$

where $p_{vapor,i}$, $p_{source,i}$, and F_i denote the vapor pressure of the source material, the pressure of the source material, and the flow through the source, respectively [29].

V/III ratio, $R_{V/III}$, indicates the ratio between the partial pressures of group V and group III source materials in the reactor and is larger than one during the growth due to the reasons explained earlier. V/III ratio is given by

$$R_{V/III} = \frac{p^*_V}{p^*_{III}}. \tag{11}$$

The compositions, x and y, of the quaternary compounds $A_xB_{(1-x)}C_yD_{(1-y)}$ depend on the ratio of the flows of different source materials. In mass-transport controlled growth, the composition, x, is simply given by

$$\frac{x}{1-x} = \frac{F_A}{F_B}, \tag{12}$$

where the F_A, F_B are the flows of the two different group III source materials. In contrast; the composition, y, is given by:

$$\frac{y}{1-y} = K\frac{F_C}{F_D}, \tag{13}$$

where the F_C, F_D are the flows of the two different group V source materials [31]. The distribution coefficient, K, is required for group V atoms because there is an excess of group V atoms inside the reactor. This coefficient is determined by the relative bond strengths of the constituting binary alloys.

3.4 Setup

All of the samples grown for this thesis were fabricated using MOVPE apparatus manufactured by Thomas Swan & Co. Ltd. The apparatus is located in the clean

room of the Micronova building, and it is comprised of the control system and the gas system. The control system is composed of the electronics, the software, and the main computer. The main computer controls the gas system, and the conditions inside the reactor during growth are defined with the growth recipe program.

The gas system, which connects the organometallic source materials through the reactor to the exhaust, is composed of gas lines, mass flow controllers (MFCs), valves, and bubblers. The schematic of the gas lines is presented in figure 12. The gas system is designed in such a way that every source material has its own gas line. These gas lines are combined just in front of the reactor to minimize the pre-reactions occuring between the different source materials. In addition to this, the gas lines are constantly purged with hydrogen or nitrogen carrier gas to prevent backflow. The fluxes of the gas flows are controlled by MFCs.

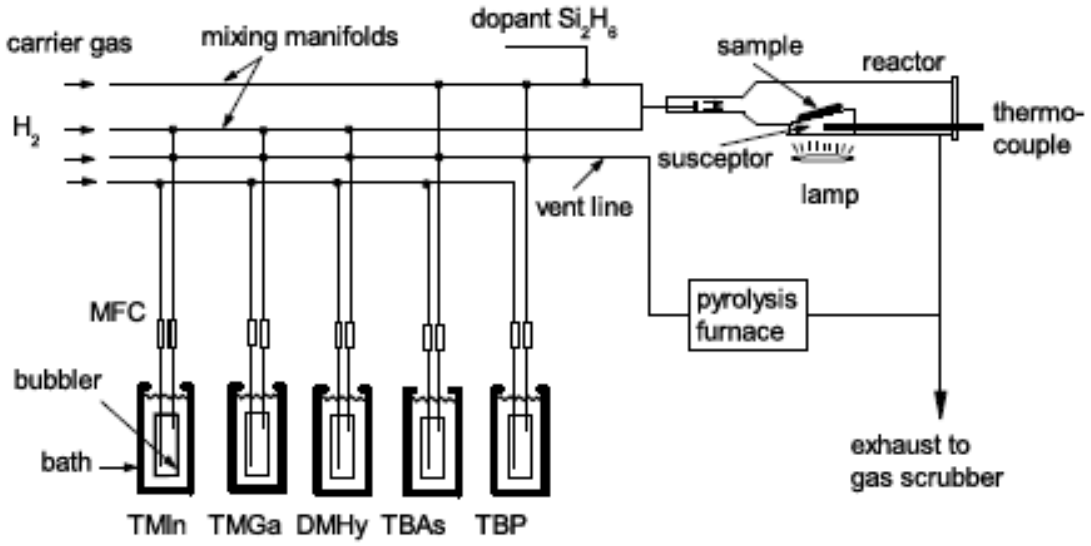

Figure 12: Schematic illustration of the MOVPE gas lines shows how the source materials are connected through the reactor to the exhaust [34]. DMHy source and dopant Si_2H_6 lines are also indicated in this figure, but they were not used in this thesis.

Organometallic source materials are inside bubblers, which are located in a liquid baths. The temperature of the baths can be controlled between -20°C and 30°C, so that a suitable vapor pressure of the source material can be chosen. When the carrier gas flows as tiny bubbles through the source material, it becames saturated (up to the vapor pressure) with the precursor. Figure 13 illustrates the operation principle of the bubbler.

Growth of III-V compound semiconductors occurs inside a quartz-glass reactor whose crossection is shown in figure 14. The shape of the reactor is designed so that the gas flow through the reactor is as laminar as possible. The substrate is placed on the top of a graphite susceptor inside the reactor. The susceptor is heated

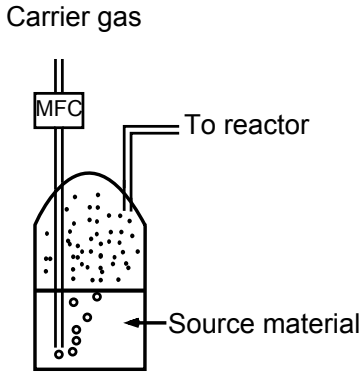

Figure 13: Carrier gas flows through the source material as bubbles where the source molecules evaporate and saturate the carrier gas.

up by an infrared lamp, which is located under the susceptor. The temperature of the susceptor is measured by a thermocouple element inside the susceptor. Therefore, the real temperature of the substrate is actually lower than the thermocouple reading because of the cooling effect of the flowing gas. All growth temperatures mentioned later in this thesis are thermocouple readings. The thermocouple is protected with a quartz-glass tube.

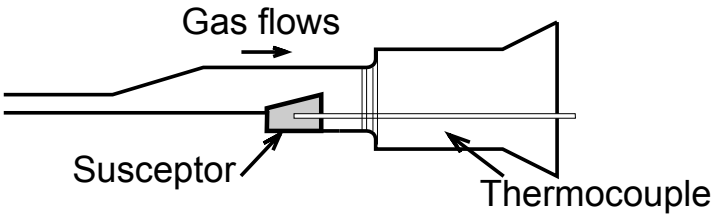

Figure 14: Crossection of the reactor shows the suscepeptor and the thermocouple. Position of the infrared lamp is under the susceptor, and is not visualized in this figure.

3.5 Growth of InP and lattice-matched InGaAsP on InP substrates and As/P exchange reaction

InP is a good substrate material for optoelectronic devices operating at near infrared wavelengths and telecommunication wavelengths. In figure 4, the band gap and the lattice constant of different III-V compound semiconductors was presented as a function of the composition. It can be observed from the figure, that the quaternary alloy $In_xGa_{(1-x)}As_yP_{(1-y)}$ can be grown on InP as lattice-matched (represented as a dashed line below InP in figure 4). The emission wavelength corresponding to the band gap can be engineered between 0.9 μm and 1.7 μm. Growth of InP based materials is a challenging task and the main difficulties encountered in their MOVPE growth are presented next.

The first difficulty in growth of InP based materials is the desorption of phosphorus at high temperatures. To reduce this desorption, lower growth temperatures could be used. However, the problem then encountered is that the pyrolysis of TBP is no more complete. Therefore, succesful growth requires either a source material for phosphorus with lower pyrolysis temperature or a scheme to compensate for the desorption of phosphorus. In general, InP materials are grown at temperatures higher than the pyrolysis temperature of TBP (550°C) with high V/III ratios. In this case, the desorption of phosphorus is no more a major problem. High partial pressure of phosphorus ensures that when a phosphorus atom is desorbed large amount of phosphorus atoms are able to replace the desorbed phosphorus atom at the surface. Usually, a V/III ratio higher than 100 is used in the growth of InP based materials.

Another difficulty is As/P exchange reaction. This reaction occurs between phosphorus and arsenic atoms when growing compounds with an arsenic component on III-phosphide surfaces. The reaction complicates the growth of these material combinations. Wang *et al.* have examined the impact on As/P exchange reaction to the growth of InAs/InP structures [32]. In their study, the morphology of InP layers was examined after annealing them under arsine flow. The examination revealed islands on the annealed InP surface. The optical properties of the annealed sample was examined by growing a capping-layer of InP on the annealed InP surface. The annealing created a shift in the luminescence peak positions of the sample. Therefore these islands can not be pure InP islands. The observed islands were suggested to be $InAs_yP_{1-y}$ material and form due to the SK growth mode of InAs on InP. The island growth was caused by the As/P exchange reaction.

In this work, the As/P exchange reaction is encountered in the growth of InAs QDs on InP or InGaAsP surfaces. In addition to this, the reaction is also occurring when growing InGaAsP on InP. In this reaction, arsenic atoms replace phosphrus atoms at the InP surface, thus causing the formation of excess InAs. This replacement occurs due to the stronger bond between indium and arsenic atoms than between indium and phosphorus atoms. As a result, phosphorus atoms are more likely desorbed from the surface than arsenic atoms. The As/P exchange reaction is encountered at temperatures above the phosphorus desorption temperature (∼360°C) [33]. The As/P exchange reaction is usually compensated by using a significantly larger TBP flow rate than the TBAs flow rate.

The effects of As/P exchange reaction on the InAs QD formation in complete SOA structures can also be suppressed by growing an ultra-thin (1-2 monolayer) interlayer of GaAs between the InGaAsP and InAs layers. Gong *et al.* have examined the effects of the GaAs interlayer on the InAs islands [14]. They discovered in their study that the GaAs layer protected the phosphorus atoms from the substitution by arsenic atoms, thus enabling better control of the InAs island structure. In addition to this, GaAs layer provided an effective mean to tune the emission wavelength of the InAs QDs and enhanced the optical properties of the sample. Therefore, an interlayer of GaAs between the InAs and InGaAsP layers could enable the SOA components to operate more efficiently.

4 Characterization methods

This chapter describes all the experimental methods used in the characterization of the samples fabricated for this thesis.

4.1 Atomic force microscopy

AFM is a high-resolution scanning method used for examination of sample morphology. AFM typically has a vertical resolution of less than 1 nm. AFM apparatus is composed of a cantilever and a tip, a laser system, a photodetector, feedback electronics, and a piezoelectric sample holder. The setup of AFM is presented in figure 15.

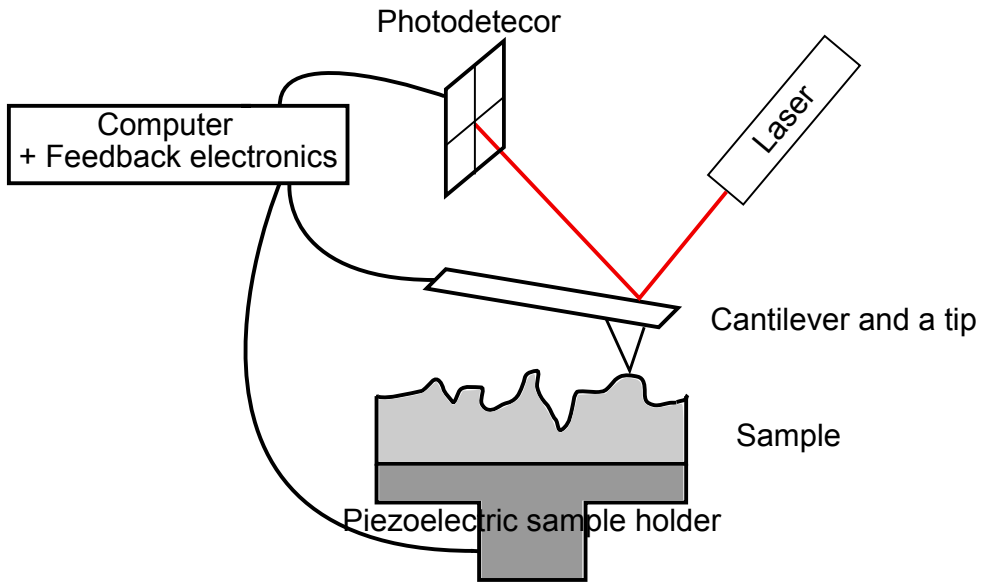

Figure 15: Schematic illustration of the operation principle of AFM.

The operation principle of AFM is based on the atomic interactions between the tip and the surface of the sample. The movement of the tip is observed by the laser system. The laser beam is reflected from the back of the cantilever to the center of the photodetector. The piezoelectric sample holder moves the sample very accurately, thus allowing the position of the sample to be controlled with nanometer precision. The AFM tip approaches the sample surface before the scan. The distance between the tip and the surface is minimal (*i.e.*, a few nanometers). Next, AFM starts to scan the sample. While scanning, the distance between the tip and the sample surface constantly changes and depends on the morphology of the sample. When the distance changes, the laser beam reflects to a different position on the photodetector. AFM attempts to maintain the reflection at a fixed point by using feedback electronics to drive the vertical direction of the piezo sample holder. The information about the sample morphology is obtained from the feedback signal.

Scanning can be performed by using two different scanning modes. In the contact mode, scanning is excecuted by raising the sample as high as the photodetector observes some movement of the reflected laser beam. In the semicontact mode, the AFM tip resonates at its own resonance frequency while scanning the sample surface. The resonance frequency of the tip depends on the distance between the sample surface and the tip. Therefore, the information about the sample morphology is obtained by maintaining the resonance frequency.

The Ntegra Aura AFM, which was used in this thesis, was manufactured by the company NT-MDT. The maximum scan size of this device was 13μm$\times 13\mu$m. The AFM apparatus was placed on a damped table during the scanning to reduce the noise originating from vibrations in the environment. All the images were taken in semicontact mode and improved using the mathematical algorithms provided by the AFM software.

4.2 Photoluminescence measurement

PL is an optical spectroscopy method used for the examination of energy states in semiconductor materials. The setup of the PL measurement is presented in figure 16. The setup is comprised of an excitation laser, a detector, a lock-in amplifier, a monochromator, a computer, a sample holder, a cryostat, a chopper, and multiple mirrors, lenses and attenuators.

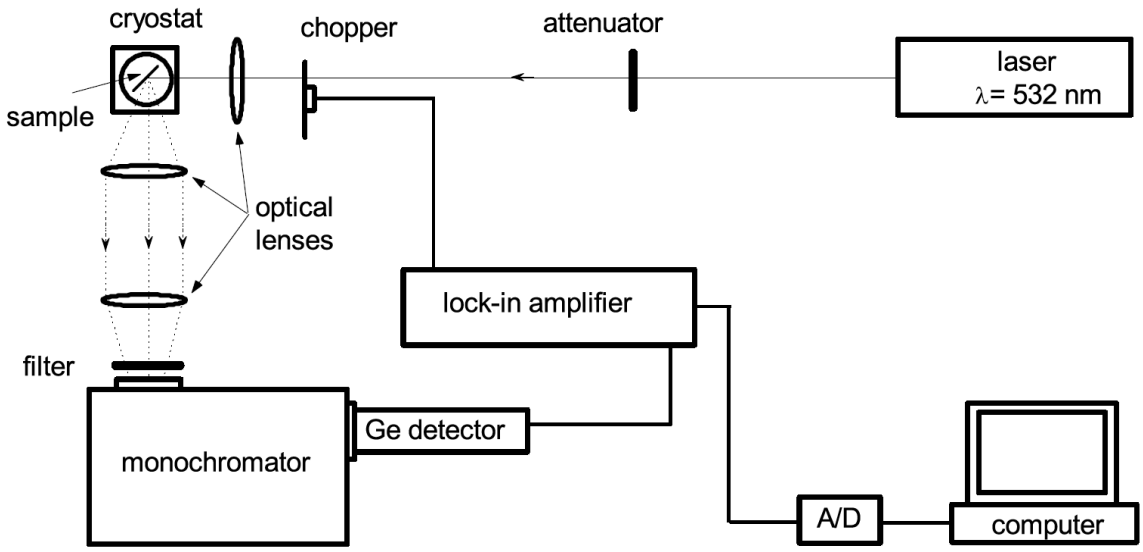

Figure 16: Setup of the PL mesurement [34].

During the measurement, the samples are placed inside the cryostat. The temperature of the cryostat can be changed between 8 K and 300 K. The excitation beam from the laser is guided through the chopper to the sample surface. The wavelength of the excitation laser should be smaller than the wavelength corresponding to the

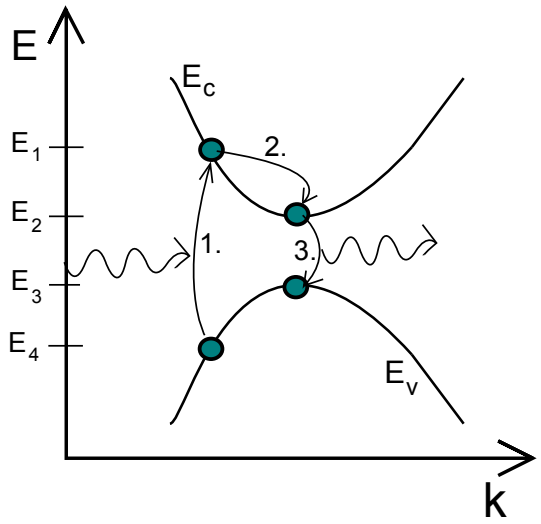

Figure 17: Principal recombination and excitation processes occurring in the PL measurement are shown in E-**k**-diagram. The processes 1, 2, and 3 in the figure describe the excitation, thermalization, and recombination processes of charge carriers, respectively. The wavelength of the exitation laser equals the corresponding wavelength of the difference between energy states E_1 and E_4. The measured PL signal equals the wavelength corresponding to the energy difference between states E_2 and E_3.

band gap of the examined material. The laser light is absorbed in the sample and excites charge carriers from the valence band to the conduction band (see figure 17). After that, the excited charge carriers thermalize to near-band-edge energy states. Then, the charge carriers recombine either radiatively or non-radiatively. The energy of the generated photons corresponds to difference between the participating states in the sample.

Emitted photons are collected to the monochromator. The reflected laser beam is filtered before it enters the monochromator. The monochromator allows only a certain wavelength of the spectrum to be transmitted through at a time. The detector is located at the output of the monocromator and measures the intensity of the transmitted photons. A lock-in amplifier is used to improve signal-to-noise ratio by phase-locking the detector output and the reference signal from the chopper. The measurement data is collected and stored in the computer.

The PL measurement was executed either at the temperature of 8 K (LT-PL) or at 300 K (RT-PL). The germanium detector was cooled down to the liquid nitrogen temperature, 77 K. A frquency doubled 532 nm Nd:YVO_4 laser was used for excitation.

4.3 X-ray diffraction

XRD is an experimental method used for the examination of the crystal structure of crystalline materials. The XRD system is comprised of a X-ray generator, mirrors, lenses, attenuators, a detector, a movable sample holder and a computer. In the XRD measurement, X-rays which are guided to the sample with mirrors and lenses hit the sample and diffract because of the periodicity of crystalline materials. The intensity of the diffracted rays is measured with the detector from different angles. Structural information of the sample can be extracted from the diffraction curve. After the diffraction curve is measured, the computer is used for fitting a known diffraction curve to the measured one. The information relating to the composition and the layer thicknesses is obtained from the fitted graph. XRD omega-2theta measurement was performed in this thesis to obtain information about the composition of the quaternary alloy InGaAsP. In this measurement, both the omega and theta angle of the apparatus were changed simultaneously to achieve the diffraction curve.

5 Results

This chapter presents and discusses all the obtained results, and is organized in the following way. Section 5.1 explains how different InAs QD samples have been fabricated. The rest of this chapter, then, presents the different characteristics of these samples. Section 5.2 explains the self-assembled growth of InAs islands on InP substrate. The optical properties of InAs QDs inside InP are presented in section 5.3. Section 5.4 discusses the tuning of the InAs QD wavelength peak in the 1.55 μm region by using a lattice-matched $In_{0.79}Ga_{0.21}As_{0.55}P_{0.45}$ quaternary alloy as an interlayer.

5.1 Fabrication of InAs QD samples

Three kinds of different InAs QD structures were fabricated for this thesis. All of the samples were grown on 500-μm-thick semi-insulating (100) InP substrates. Before growth, the substrates were cleaned chemically in the following way. Substrates were dissolved in acetone for two minutes and in isopropanol for two minutes. During this, the samples and the chemicals were placed in ultrasonic sinc. Then, the samples were flushed by de-ionized water for five minutes. After this, substrates were blow-dried with N_2 and placed on the susceptor inside the MOVPE apparatus.

In the first series of samples, a 100-nm-thick InP buffer layer was grown on the substrate with a V/III ratio of 220, a growth temperature of 640°C, and a growth time of 450 s. Then, InAs island layer was grown on the InP buffer layer with a V/III ratio of 12. The growth temperature and growth time of this layer were changed between 420°C and 550°C, and between 1.25 s and 8.25 s, respectively. The schematic structure of these samples is shown in figure 18a

In the second series of samples, a 100-nm-thick InP buffer layer was grown on the substrate with the same growth parameters as in the first samples. Then, an InAs layer was grown on the InP buffer layer at the temperature of 520°C. The growth time of the layer was between 1.25 s and 10.6 s. After this, the InAs layer was capped with a 50-nm-thick InP layer. The InP capping layer was grown at the same temperature as the InAs layer. This was performed to avoid unnecessary temperature ramping which was evaluated to cause more harm than the relatively low growth temperature of InP. The schematic structure of these samples is shown in figure 18b.

In the third sample set, a 100-nm-thick InP buffer layer was again grown with the same growth parameters as in the previous samples. Then, a 100-nm-thick $In_xGa_{1-x}As_yP_{1-y}$ barrier layer was grown on the InP barrier layer with a V/III ratio of 120, a growth temperature of 640°C and a growth time of 350 s. The aim was to grow the InGaAsP layer as lattice-matched to InP as possible. The distribution coefficient, K, of equation 13 was evaluated to be 6.3 based on the XRD and PL measurement results. After this, the InAs QD layer was grown on InGaAsP at 520°C with a V/III ratio of 12 and a growth time of 2 s. Then, this InAs layer

was capped with a 50-nm-thick $In_xGa_{1-x}As_yP_{1-y}$ layer. This layer was grown at the same temperature as the InAs layer due to the reasons described earlier. One sample was grown without a capping layer for the examination of the morphology of the InAs layer on $In_xGa_{1-x}As_yP_{1-y}$. The schematic structure of these samples is shown in figure 18c

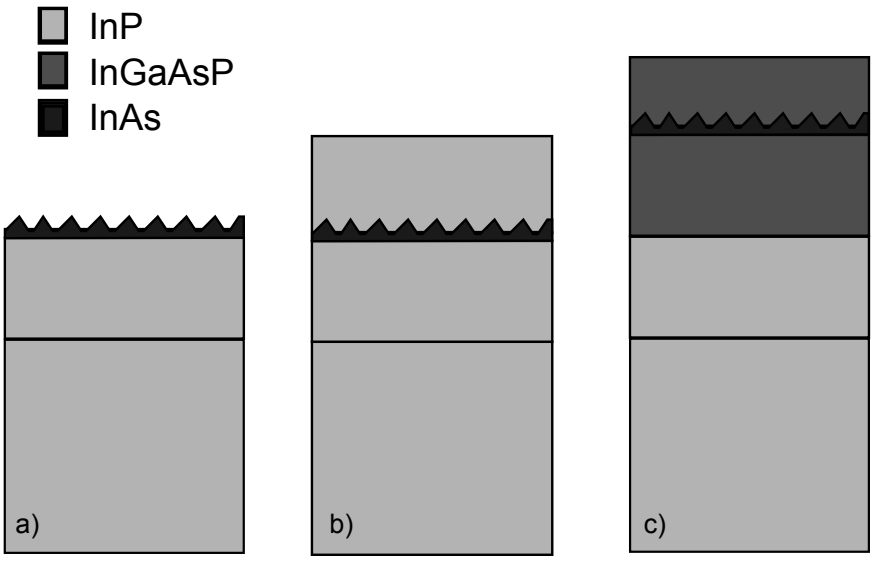

Figure 18: Crossection of the fabricated samples: (a) InAs/InP island structure, (b) InAs/InP QD structure, and (c) InAs/InGaAsP/InP QD structure.

5.2 Self-assembled growth of InAs islands on InP

Self-assembled growth of InAs islands on InP was examined by fabricating two series of samples (structure of figure 18a). The nominal thickness and growth temperature of the InAs layer were varied in these series. In the first series, the nominal thickness of the InAs layer was varied from 1 monolayer (ML) to 6 MLs. The growth temperature of the InAs layer was 500°C. The sample morphology was examined by AFM. Figure 19 shows the AFM images taken from this series.

In figure 19, the transformation from 2D layer to 3D island growth mode is clearly observed. The first deposited InAs ML is a smooth 2D surface. This 2D layer is a direct evidence of the InAs WL. The first InAs islands start to be form when the nominal thickness of InAs exceeds 1.6 MLs resulting in very flat InAs islands. Diameter of these islands is approximately 100 nm and the height at most a few nanometers. Larger InAs islands are observed when the nominal InAs thickness is above 3 MLs. The formation of the InAs islands verifies the SK growth mode of InAs on InP. Areal island densities and average heights of the islands were calculated for InAs layers with a nominal thickness larger than 3 ML. The values for island densities are 2.3×10^9 cm^{-2}, 1.5×10^{10} cm^{-2}, and 2.5×10^9 cm^{-2} for 3-ML-thick, 4-ML-thick,

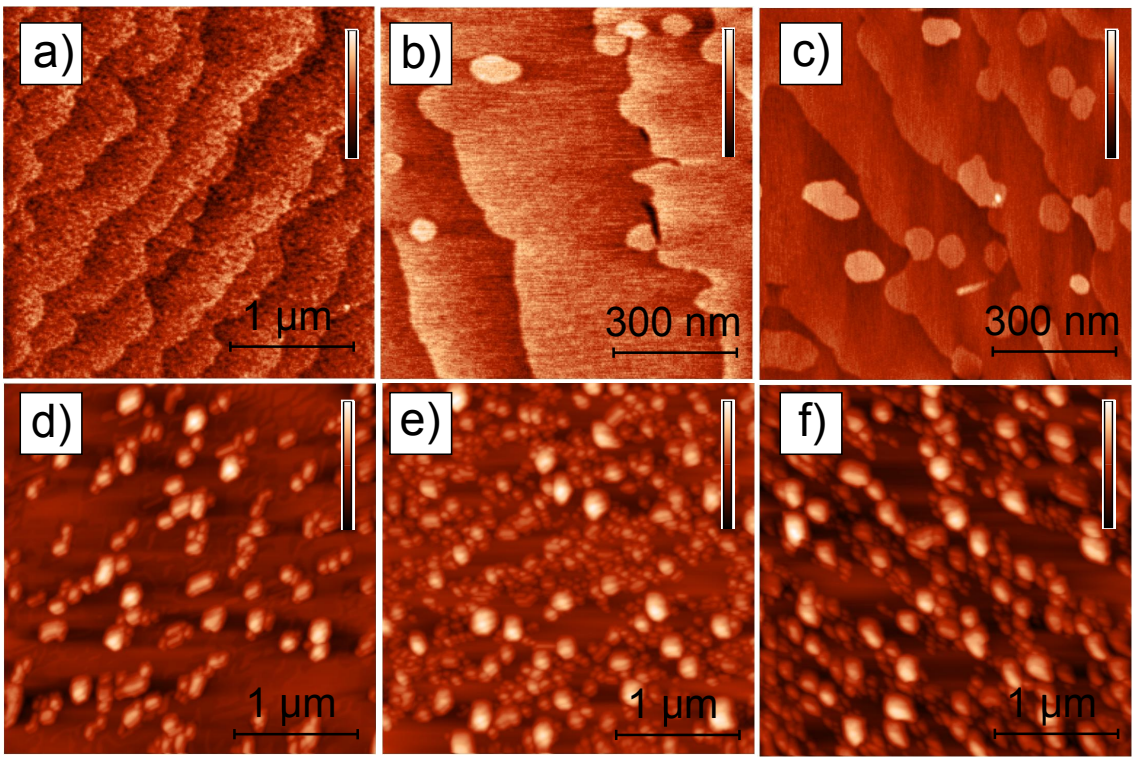

Figure 19: AFM images from the InAs/InP samples grown with the nominal thickness of (a) 1ML, (b) 1.6 ML, (c) 2 ML, (d) 3 ML, (e) 4 ML, and (f) 6 ML. Samples were grown at 500°C. The color scale of the image corresponds to the height of: (a) 1,5 nm, (b) 1 nm, (c) 2 nm, (d) 45 nm, (e) 45 nm, and (f) 55 nm.

and 6-ML-thick InAs layers. In addition, the average heights of the islands were 6 nm, 10 nm, and 12 nm, respectively.

Ponchet *et al.* have also examined the relation between the nominal InAs thickness and the InAs layer structure [12]. They studied a series of samples having an InAs layer grown on InP by MBE. The InAs layer had a nominal thickness of 1.5 ML, 1.8 ML, 2.5 ML, or 4 ML. In addition, the InAs surface was annealed for 30 seconds under the partial pressure of arsine which allowed islandation to proceed even further by the As/P exchange reaction. After this, a 25-nm-thick InP capping layer was grown on InAs islands. The structural properties of InAs islands were examined by transmission electron microscopy (TEM). TEM examination revealed that InAs islands were formed with the island densities of 0.17×10^{9} cm^{-2}, 1×10^{9} cm^{-2}, 1.1×10^{10} cm^{-2}, and 2.8×10^{10} cm^{-2} for the nominal InAs thickness of 1.5 ML, 1.8 ML, 2.5 ML, and 4 ML, respectively. It seems quite clear that 1.5 ML is near the critical thickness for the transformation of 2D to 3D growth mode. The island density increases by a decade between the nominal thicknesses of 1.5 ML and 1.8 ML. Otherwise, the results are similar in this work, but the island density decreased by a decade when increasing the thickness from 4 ML to 6 ML. Ponchet *et al.* also reported that the average height of InAs islands decreased when the InAs nominal thickness was increased from 1.8 ML to 4 ML. This is also in contradiction to the

results of this thesis. Ponchet *et al.* explained their results suggesting that the large islands evolve into the smaller islands. They argued that this evolving process occurs because the island esemble attempts to minimize its energy. They claimed that at large island densities the large islands are located too closely for them to relax their strain energy via substrate deformation. Small islands require less space for strain relaxation through the substrate; and therefore, large islands are evolving into smaller islands.

The explanation suggested by Ponchet *et al.* could also explain the results presented in this thesis. Then, the differences in the results originate from the different stage of the island formation. The decrease in the island density between the 4 ML and 6 ML can be caused by the fact that the surface is so densely occupied by the large InAs islands that these islands are not capable of relaxing their strain energy. This leads to the coalescence of islands and formation of dislocations. As a result, the island density decreases and the island size increases. It is possible that the coalescence has already started in the 4 ML sample because the size distribution of the InAs islands looks bimodal.

Bansal *et al.* have examined similar structural characteristics of the InAs layer [13]. In their study, InAs layer was grown on InP substrate by MOVPE. The growth temperature was 450°C and the nominal thickness of the InAs layer was between 4.5 ML and 9 ML. The results concur with the ones presented in this thesis. However, the transformation from 2D to 3D growth mode occurs at 4.5 ML. This difference can be explained by the lower InAs growth temperature which supresses the effects of As/P exchange reaction, thus decreasing the growth rate of InAs.

The effect of the InAs growth temperature on the morphology of the InAs islands was examined by fabricating another series of samples. The nominal thickness of the InAs layer was 3 ML. The growth temperature of InAs was varied between 450°C and 550°C. Figure 20 shows the AFM images taken from these samples (AFM image of the 450°C sample is not shown). No clear InAs islands are observed when the growth temperature is below 500°C. Small islands are observed when the InAs growth temperature is 500°C. Larger InAs islands are observed when the growth temperature is increased. Figure 21 presents the relationship between the InAs island density, the average height of the island, and the growth temperature.

Usually, the increase in the island growth temperature results in the formation of bigger islands and a decrease in the island density because the mobility of the adsorbed atoms is increased with increasing growth temperature. This kind of behaviour is observed, especially, in InAs/GaAs islands [35]. Based on figure 20, the increase in the island growth temperature does not result in a smaller island density. No InAs islands are observed when the growth temperature is less than 500°C. Taskinen *et al.* have also observed similar behaviour [8]. They used a nominal thickness of 2 ML and suggested that this behaviour is due to the fact that the mobility of surface atoms or the InAs layer thickness is too small for transformation from 2D growth mode to 3D growth mode.

The differences between InAs/GaAs and InAs/InP islands are better explained by

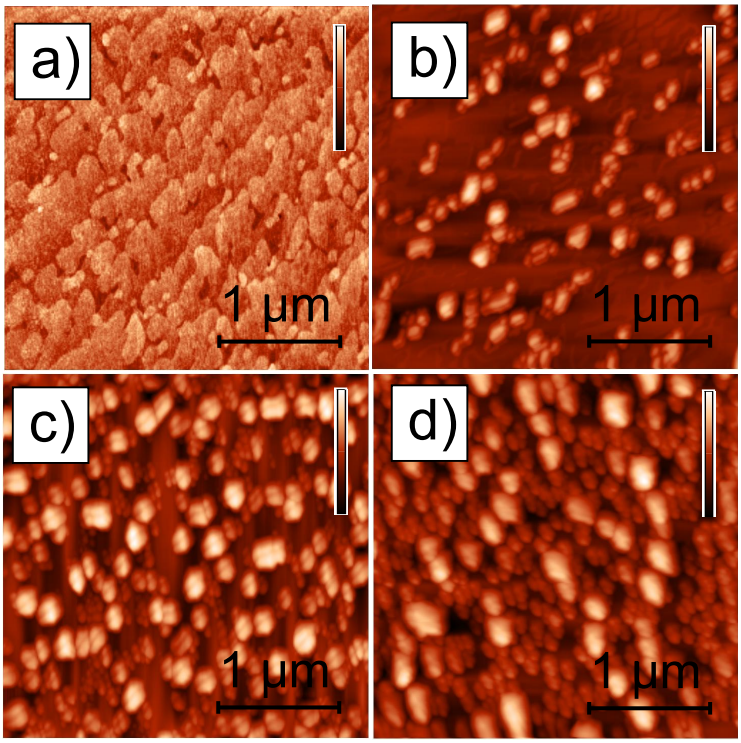

Figure 20: AFM images from the InAs/InP samples grown at (a) 480°C, (b) 500°C, (c) 520°C, and (d) 550°C. The color scale of the image corresponds to the height of: (a) 2 nm, (b) 45 nm, (c) 50 nm, and (d) 80 nm.

the generation of excess InAs material resulting from the As/P exchange reaction. This reaction is not encountered in InAs/GaAs material system. The reaction is stronger at higher growth temperatures [32]. Therefore, the growth rate of InAs is higher at higher temperatures. In addition, the cooling down process also affects the island formation. Samples are cooled down under TBAs partial pressure. Therefore, the As/P exchange reaction forms islands even after the TMIn flow has stopped.

5.3 Optical properties of InAs/InP QDs

The optical properties of InAs QDs were examined by fabricating a series of samples where InAs islands were capped by InP. In this series, the nominal thickness of InAs was between 0.9 ML and 8 MLs. The InP capping layer was 50 nm thick. The structure of these samples was presented in figure 18b. The optical properties of InAs QDs were examined by LT-PL measurement. LT-PL results are presented in figure 22. The experimental observations can be summarized as follows:

1. The PL peak at 918 nm is observed in every sample. This peak is due to near-band-edge transitions in InP.

2. The PL peak at 1060 nm is observed in samples where the nominal thickness

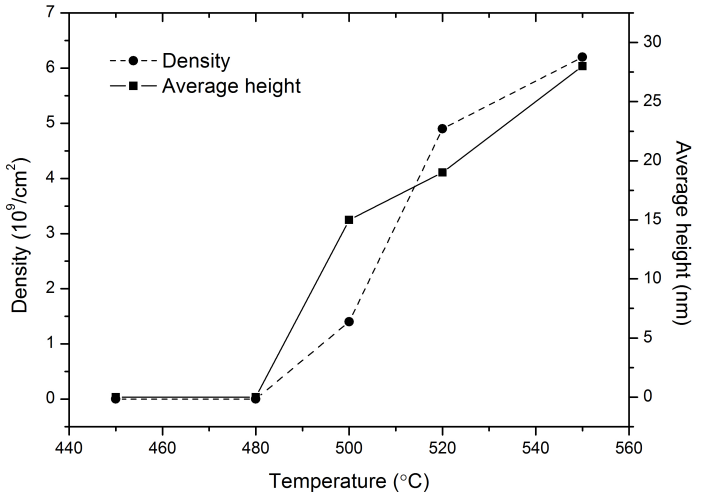

Figure 21: Height and density of the InAs islands as a function of InAs growth temperature.

of InAs is less than 2.6 nm. This PL peak is generated by the InAs WL. The band gap of InAs is 0.354 eV which corresponds to an infrared wavelength of 3500 nm. However, InAs WL is in practse a very narrow QW and, therefore, the bound energy states locate very near the band edge of the barrier.

3. The PL peak located between the wavelengths of 1060 nm and 1200 nm is observed in samples where the InAs nominal thickness is 1.4 ML and 2 ML. These peaks are attributed to transitions originating from InAs. The luminescence corresponds to either another WL transition or to small InAs QDs. This will be discussed more later. The intensity of the PL peak in the sample with nominal InAs thickness of 2 ML is extremely high. The PL peak is located at 1160 nm and has a full-width-at-half-maximum (FWHM) of 50 nm.

4. The broad PL peak located at the wavelengths of beyond 1400 nm is observed in samples where the InAs nominal thickness exceeds 3 ML. This PL peak is attributed to transitions inside larger InAs QDs. It should be taken into account that the response of the used germanium detector degrades above the wavelength of 1.65 μm.

5. The PL peak at 980 nm is observed in the sample with nominal InAs thickness of 2.6 ML. It seems possible that this peak is caused by the WL, which already has a reduced thickness compared to that of the 2-ML-thick InAs. This would indicate that the formation of larger 3D islands has just started in the sample. However, due to the very low areal density of the dots, the luminescence intensity at above 1400 nm is still too weak to be seen.

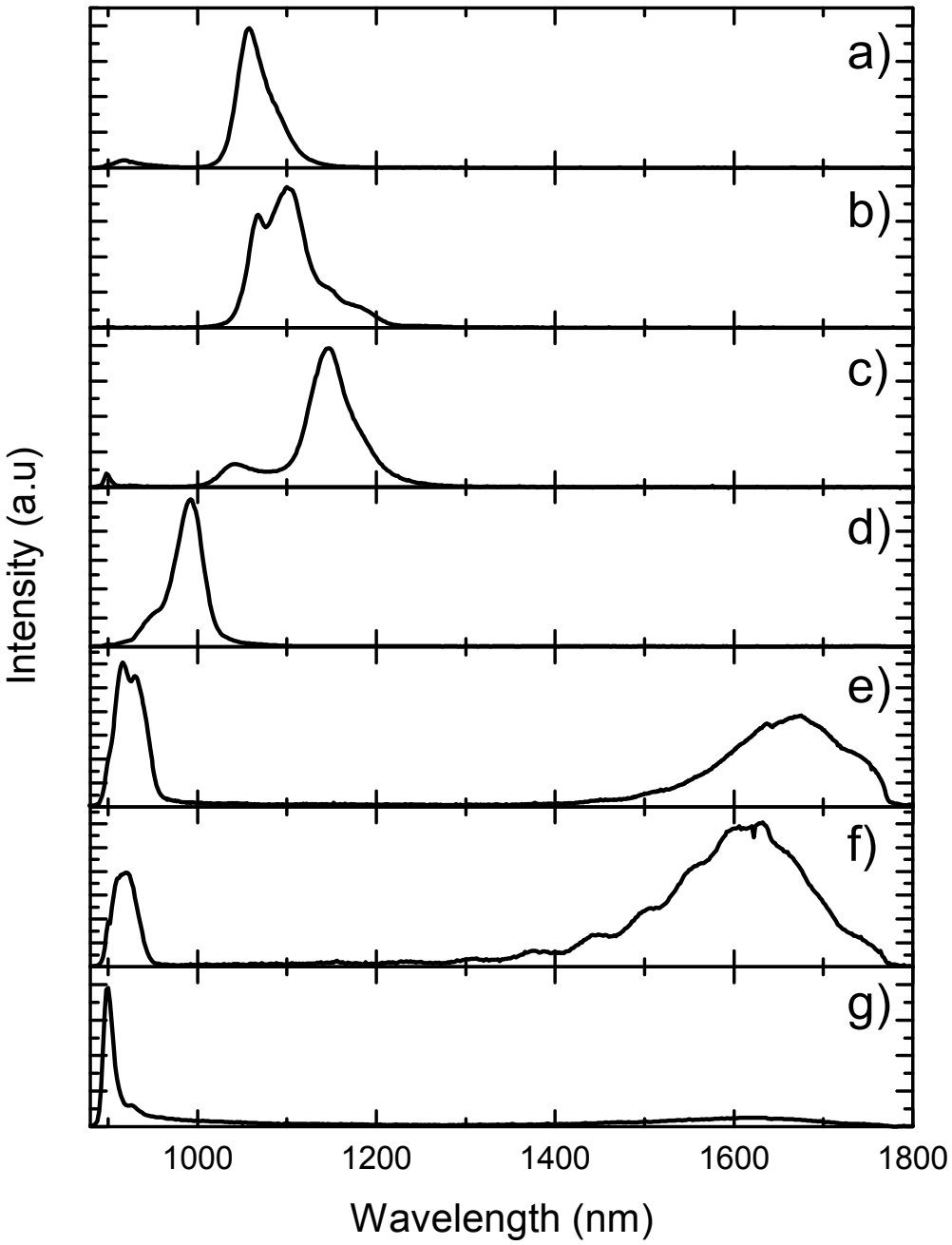

Figure 22: LT-PL spectra from InP/InAs/InP structures having a nominal InAs thickness of (a) 0.9 ML, (b) 1.4 ML, (c) 2 ML, (d) 2.6 ML, (e) 3.2 ML, (f) 4 ML, and (g) 8 ML. InAs layer was grown at 520°C.

Taskinen *et al.* have also examined the optical properties of the capped InAs islands [8]. They observed similar characteristics in their study. They attributed the PL peaks between 1400 nm and 1800 nm to originate from the transitions of InAs QDs. In addition, PL peaks at wavelengths less than 1400 nm were attributed to

transitions inside the WL. They detected two WL-related PL peaks and suggested that these peaks are due to the variations in the WL thickness. To support their claim, they calculated the theoretical transition energies between the conduction band and the valence band of a strained InAs/InP QW. In their calculations, a QW with 2 ML and 3 ML thickness produced energy transitions of 1.2 eV and 1.1 eV, respectively. This corresponds to a wavelength of 1040 nm and 1130 nm, and is therefore near the locations of the PL peaks described in observations 2-3. The relation between the InAs growth thickness and the optical properties is also examined by Murray *et al.* [11]. A different explanation was suggested for the origin of the two WL-related PL peaks. PL peaks were attributed to occur due to the differences in the composition of the WL. The composition of the WL is actually $InAs_yP_{1-y}$ because of the As/P exchange reaction.

Both of these explanations can specify the origin of the PL peaks in observations 2 and 3 presented earlier. To examine the origin of the peaks an AFM image was taken from the uncapped sample with InAs nominal thickness of 2 MLs. AFM image is shown in figure 23. InAs islands are clearly observed in this image. InAs islands have an average diameter of 70 nm and an average height of 10 nm. Therefore, this would indicate that the PL peak from the samples with nominal InAs thickness of 2 ML originates from the InAs QDs. However, the island structure in an uncapped sample is not similar to that of the capped sample because of the As/P exchange reaction. The uncapped samples are cooled down under TBAs partial pressure and, therefore, the excess InAs material is actually generated in uncapped samples. As a result of this, the QDs must be smaller or there are no islands in the capped samples. Therefore, this observation does not completely verify the origin of the PL peak in observation 3. To fully understand the origin of these PL peaks, further examination is necessary. For instance, TEM could give more information about the structure of the InAs layer in the capped sample.

5.4 Tuning the QD peak position to 1,55 μm with InGaAsP

Waveguide-like structure, which maintains the optical signal inside the amplifying region, *i.e.*, near the QDs, is required for the operation of SOA. One way to accomplish this is to utilize the total internal reflection between the two media with different refractive indices. Fabricating InAs QDs inside the quaternary compound InGaAsP, and this inside InP allows the InGaAsP layer to form a waveguide structure which keeps the optical mode near the InAs QDs. One extra advantage that is gained from this is the possibility to redshift the wavelength of the QD PL peak. The redshift occurs due to the change in the height of the potential barrier experienced by the charge carriers in the dots. This section examines the tuning of the InAs QD PL peak to telecommunication wavelengths and presents the opical and structural properties of the InAs/InGaAsP/InP QD structure. The lattice-matched quarternary alloy $In_{0.94}Ga_{0.06}As_{0.17}P_{0.83}$ was grown on InP as a waveguide media. This composition was chosen because it has the band gap of 1.22 eV which was estimated to redshift the QD PL peak to the telecommunication wavelengths. The

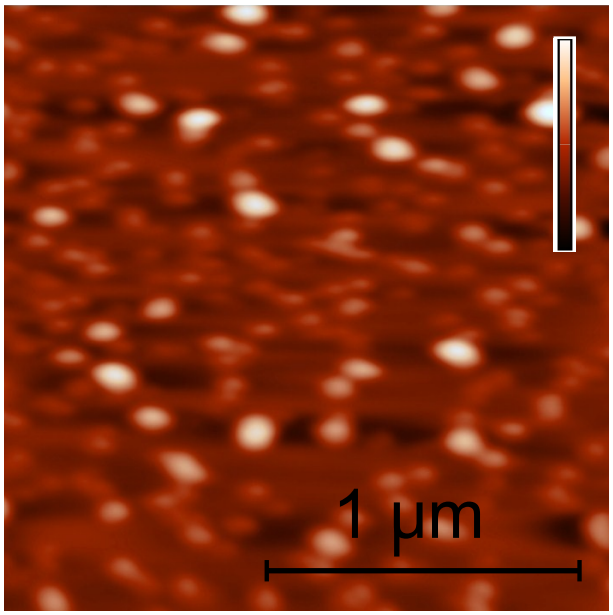

Figure 23: AFM image of the uncapped InAs islands grown on InP at 520°C with the nominal InAs thickness of 2 ML. The color scale of the image corresponds to the height range of 35 nm.

structure of the samples was presented in figure 18c.

The lattice-matching between InGaAsP and InP was examined by XRD measurement of a separate sample where a 100-nm-thick bulk InGaAsP layer was grown on InP. Figure 24 presents the measured omega-2theta XRD curve of this sample. The XRD peak at -500 arcsecs from the InP peak is due to the InGaAsP layer. This peak confirms the near-perfect lattice-mathing between the $In_{0.94}Ga_{0.06}As_{0.17}P_{0.83}$ and InP layers.

Formation of InAs islands on lattice-matced InGaAsP layer was examined by fabricating InAs islands on InGaAsP without InGaAsP capping layer. The InAs islands were grown at 520°C with a nominal thickness of 2 ML. The AFM image from the sample is presented in figure 25. Quite homogeneous InAs islands were observed on the sample surface. InAs islands have an average diameter of 30 nm and an average height of 10 nm. The formation of InAs islands on InGasAsP layer differs from the formation on InP layer. This can be seen by comparing the AFM images in figures 23 and 25. The InAs layers were grown under the same conditions in both cases. The difference between these two samples indicates that the different strain conditions of the InAs/InGaAsP and InAs/InP structures play an important role in the InAs island formation. Although InP and InGaAsP compounds are nearly lattice-matched some differences in strain conditions always occur because of the different thermal expansion coefficients of the compounds. Therefore, it seems that more homogenous InAs islands can be fabricated on InGaAsP than on InP layers.

The optical properties of the InAs QDs were examined fabricating a sample where InAs QDs were capped with a 50-nm-thick $In_{0.94}Ga_{0.06}As_{0.17}P_{0.83}$ layer. Figure 26

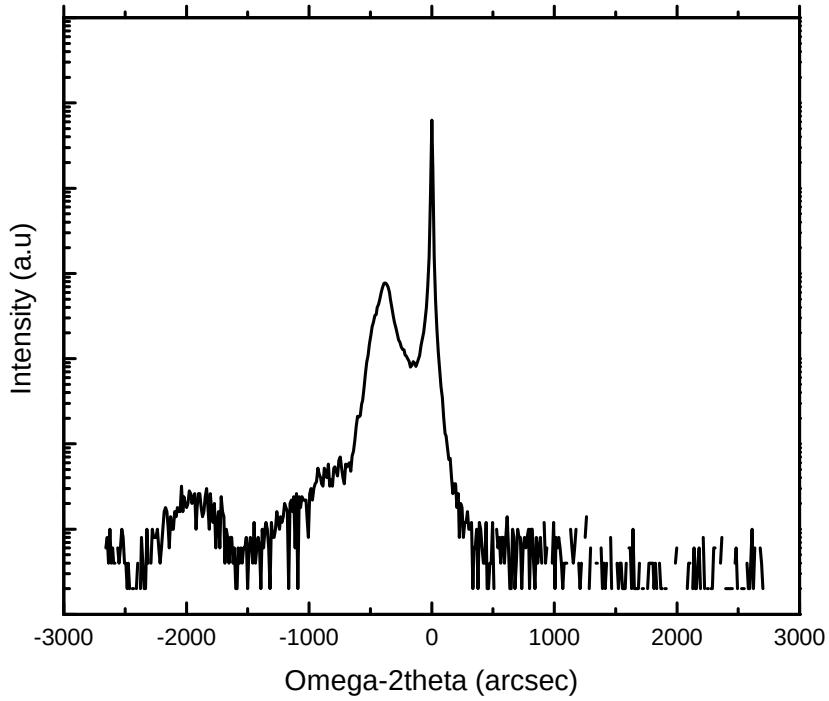

Figure 24: Measured omega-2theta XRD curve of the InGaAsP/InP layer structure.

presents the LT-PL results. Two PL peaks at the wavelengths of 1020 nm and 1560 nm are observed in the spectrum. The PL peak at 1020 nm is originated from the InGaAsP layer. The peak is very sharp and has a FWHM of 10 nm. The peak at 1560 nm originates from InAs QDs and has a FWHM of 40 nm. The RT-PL measurement results of this sample are shown in figure 27. The RT-PL signal was very noisy and it has been smoothened. A RT-PL measurement reveals a broad PL peak at the wavelength of 1060 nm. This peak is due to the InGaAsP bulk material. PL signal from the quantum dots cannot be resolved.

Jeong *et. al* have also examined the optical properties of InAs/InGaAsP/InP QDs by PL at different temperatures [9]. In their study, the samples had luminescence between 1200 nm and 1600 nm. The PL peak of the InGaAsP waveguide layer was located at 1100 nm. They observed that the integrated intensity of the InAs QD PL peak at the wavelength of 1400 nm remained very high at room temperature (20% of the value at 10 K). In addition to this, Jeong *et al.* also measured the life time of the PL transition from the QDs by time-resolved PL measurement to be 4 ns indicating that there are no significant non-radiative routes for the charge carriers.

The QD luminescence inefficiency of the structure fabricated here can be explained by many factors. It could originate from reactor contamination (there has been other indications of this during this work), too low QD density, too high dislocation density

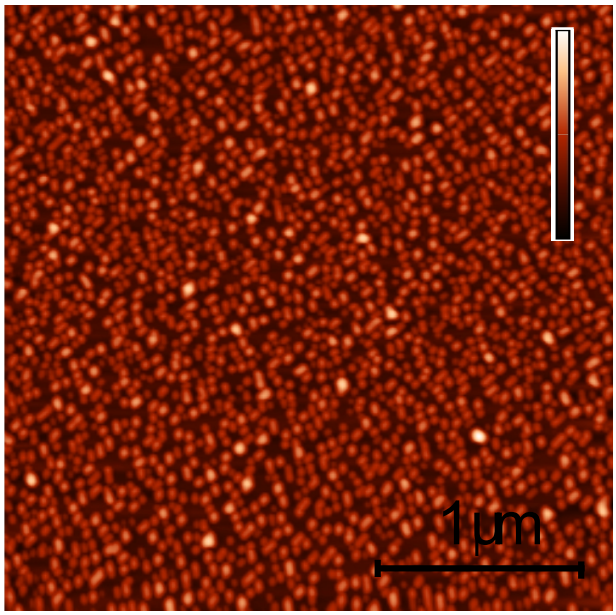

Figure 25: AFM image of the uncapped InAs islands grown on InGaAsP at 520°C with 2 ML nominal thickness. The color scale of the image corresponds to the height range of 25 nm.

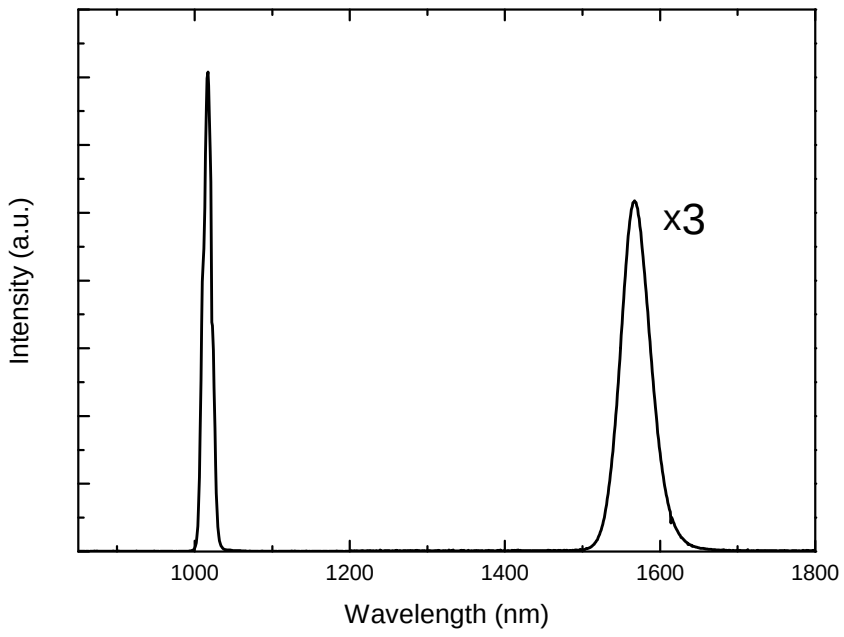

Figure 26: LT-PL spectrum of the InAs/InGaAsP/InP QD structure. The intensity level of the PL peak at 1560 nm has been multiplyed by a factor of three.

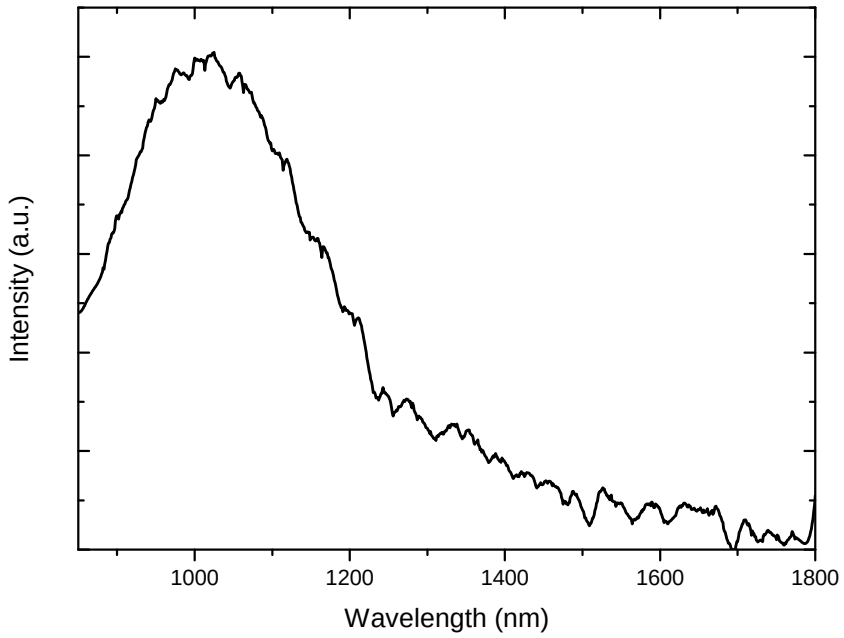

Figure 27: RT-PL spectrum of the InAs/InGaAsP/InP QD structure.

caused by the relaxed islands, or even by enhanced phonon bottleneck phenomenon (see section 2.2.2) due to deeper potential of the QDs compared to Jeong *et. al.* Therefore, more work is still required to enhance the QD luminescence intensity. For instance, the reduction of non-radiative recombination channels, the increased QD density, the fine-tuned InAs thickness, and also maybe the change in the composition of the InGaAsP waveguide layer could solve this problem.

6 Conclusions

The fabrication of InAs QD structures on InP substrates was examined in this thesis. The focus of this work was to fabricate such a structure that can be used in a telecommunication wavelength semiconductor optical amplifiers.

First, self-assembled growth of InAs islands was examined on InP substrates. The SK growth mode of the InAs/InP structure was observed. The effect of InAs growth temperature on the island structure was examined, and it was observed that the growth temperature affects the growth rate of InAs significantly. This phenomenon was attributed to the As/P exchange reaction. It was also observed that the InAs islands were not formed when using growth temperatures lower than 500°C and the nominal InAs thickness of 3 ML.

LT-PL measurement was performed for the examination of the optical properties of the InAs QDs with different nominal thickness. PL peaks were observed at the wavelength of 918 nm, 1060nm, between 1060 nm and 1200 nm and beyond 1400 nm. These peaks were attributed to energy states corresponding to the band gap of InP substrate, the InAs WL, small InAs QDs (or thick InAs WL), and large InAs QDs, respectively. Previously, it has been suggested that WL can form several PL peaks [8, 11]. In these studies, these WL PL peaks were attributed either to the variations in the thickness or to the composition of the WL. PL peaks at these wavelengths were also observed in this thesis (peaks between 1060 nm and 1200 nm). To study the origin of these PL peaks an AFM examination was performed for a similar, but uncapped, sample. This examination revealed InAs islands on InP surface. This would indicate that these PL peaks are due to the small InAs QDs. However, the As/P exchange reaction plays a significantly larger role in uncapped samples; and therefore, the origin of the PL peak was not completely verified.

To tune the InAs QD wavelength peak to telecommunication wavelengths InAs/ InGaAsP/InP QD structure was fabricated. Self-assembled growth of InAs islands was examined on an InGaAsP layer lattice-matched to InP. Based on the AFM examinations, homogenous InAs islands with an average diameter of 30 nm and an average height of 10 nm were formed. The PL results revealed that this structure emits in the 1.55 μm wavelength region.

This research can be continued to fine-tune the structure to eventually fabricate an operating InAs QD SOA. In order to perform this, the following factors still need to be solved. The material quality has to be improved to reduce non-radiative recombination at room temperature. The optimal combination of the InGaAsP composition and the InAs QD size has to be found to maximize the luminescence efficiency. The growth of the doped InP bulk layers and cleanroom processing is also required for the fabrication of a pn-junction with electric contacts. However, the SOA structure is so similar to that of InGaAsP diode laser that this should not pose unsurmountable problems.

References

[1] M. Wasfi , Optical fiber amplifiers-review, International Journal of Communication Networks and Information Security, (2009), vol. 1, pp. 42-47.

[2] R.J. Mears and S R. Baker, Erbium fibre amplifiers and lasers, Optical and Quantum Electronics, (1992), vol. 24, pp. 517-538.

[3] N. A. Olsson, Semiconductor optical amplifiers, Proceedings of the IEEE, (1992), vol. 80, pp. 375-382.

[4] J. C. Simon, GaInAsP semiconductor laser amplifiers for single-mode fiber communications, Journal of Lightwave Technology, (1987), vol. LT-5, pp. 1286-1295.

[5] M. A. Newkirk, B. I. Miller, U. Koren, M. G. Young, M. Chien, R. M. Jopson, and C. A. Burrus, 1.5 μm Multiquantum-Well Semiconductor Optical Amplifier with Tensile and Compressively Strained Wells for Polarization-Independent Gain, IEEE Photonics Technology Letters, (1993), vol. 4, pp. 406-408.

[6] H. Saito, K. Nishi, and S. Sugou, Ground-state lasing at room temperature in long-wavelength InAs quantum-dot lasers on InP(311)B substrates, Applied Physics Letters, (2001), vol. 78, pp. 267-269.

[7] A. Bilenca, R. Alizon, V. Mikhelashvili, G. Eisenstein, R. Schwertberger, D. Gold, J. P. Reithmaier, and A. Forchel, InAs/InP 1550 nm quantum dash semiconductor optical amplifiers, Electron Letters, (2002), vol. 38, pp. 1350-1351.

[8] M. Taskinen, M. Sopanen, H. Lipsanen, J. Tulkki, T. Tuomi, and J. Ahopelto, Self-organized InAs islands on (100) InP by metalorganic vapor phase epitaxy, Surface Science, (1997), vol. 376, pp. 60-68.

[9] Weon G. Jeong, P. Daniel Dapkus, U. H. Lee, J. S. Yim, D. Lee, and B. T. Lee, Epitaxial growth and optical characterization of InAs/InGaAsP/InP self-assembled quantum dots, Applied Physics Letters, (2001), vol. 78, pp. 1171-1173.

[10] N. I. Cade, H. Gotoh, H. Kamada, H. Nakano, S. Anantathanasarn, and R. Notzel, Optical characteristics of single InAs/InGaAsP/InP (100) quantum dots emitting at 1.55 μm, Applied Physics Letters, (2006), vol. 89, DOI: 10.1063/1.2378403.

[11] R. Murray, C. Bryan, C. Button, D. Spikes, and G. Hill, 1.55 micron emission from InAs/InP Self-assembled quantum dots, Materials Research Society, (2000), pp. 159-164.

[12] A. Ponchet, A. Le Corre, H. L'Haridon, B. Lambert, and S. Salaun, Relationship between self-organization and size of InAs islands on InP(001) grown by

gas-source molecular beam epitaxy, Applied Physics Letters, (1995), vol. 67, pp. 1850-1852.

[13] B. Bansal, M. R. Gokhale, A. Bhattacharya, and B. M. Arora, InAs/InP Quantum dots with bimodal size distribution: Two evolution pathways, Journal of Applied Physics, (2007), vol. 101, DOI: 10.1063/1.2710292.

[14] Q. Gong, R. Notzel, P. J. van Veldhoven, T.J. Eijkemans, and J.H. Wolter, Wavelength tuning of InAs quantum dots grown on InP (100) by chemical beam epitaxy, Applied Physics Letters, (2004), vol. 84, pp. 275-277.

[15] Connexions web library, Cited 7.1.2010, Available at http://cnx.org/content/m16927/latest/.

[16] Web site, cited 7.1.2010, Available at http://www.ecse.rpi.edu/ schubert/Light-Emitting-Diodes-dot-org/chap12/F12-06%20III-V%20bandgap%20energie.jpg, The research group of E. Fred Schubert at Rensselaer Polytechnic Institute.

[17] J. Singh, Physics of Semiconductors and Their Heterostructures, United States, McGrarw-Hill, 1993.

[18] L. Banyai and S.W. Koch, Semiconductor Quantum Dots vol 2., Singapore, 1994.

[19] H. Temkin, G.J. Dolan, M.B. Panish, and S.N.G.Chu, Low temperature photoluminescence from InGaAs/InP quantum wires and boxes, Applied Physics letters, (1987), vol. 50, pp. 413-415.

[20] K. Kash, A. Scherer, J.M. Worlock, H.G. Craighead, M.C.Tamargo, Optical spectroscopy of ultrasmall structures etched from quantum wells, Applied Physics letters, (1986), vol. 49, pp. 1043-1045.

[21] B.I. Miller, A. Shahar, U. Koren, and P.J. Corvini, Quantum wires in InGaAs/InP fabricated by holographic photolithography, Applied Physics letters, (1989), vol. 54, pp. 188-190.

[22] D. Bimberg, V.A.Shchukin, N.N. Ledentsov, A.Krost, and F.Heinrichsdorff, Formation of self-organized quantum dots at semiconductor surfaces, Applied Surface Science, (1998), vol. 130-132, pp. 713-718.

[23] U. Bockelmann and G. Bastard, Phonon scattering and energy relaxation in two-, one-, and zero-dimensional electron gases, Physical Review B, (1990), vol. 42, pp. 8947-8951.

[24] H. Benisty, C.M. Sotomayor-Torres, and C. Weisbuch, Intrinsic mechanism for the poor luminescence properties of quantum-box systems, Physical Review B, (1991), vol. 44, pp. 10945-10948.

[25] J. Urayama, T.B. Norris, J.Singh, and P. Bhattacharya, Observation of Phonon Bottleneck in Quantum Dot Electronic Relaxation, Physical Review Letters, (2001), vol. 86, pp. 4930-4933.

[26] RP photonics web library, Cited 19.1.2010, Available at http://www.rp-photonics.com/semiconductor_optical_amplifiers.html, Rudiger Paschotta.

[27] G. B. Stringfellow, Organometallic vapor phase epitaxy: Theory and Practice, ACAdemic Press, Inc., San Diego, 1989.

[28] M.G. Jacko and S.J.W. Price, Pyrolysis of trimethylindium, Canadian journal of chemistry, (1964), vol. 42, pp. 1198-1205.

[29] M. Taskinen, Fabrication of Indiumphosphide based quantum well laser, Master thesis, Teknillinen korkeakoulu, Teknillinen fysiikka, Finland, Espoo, 1994.

[30] K. Tu, J.W. Mayer, L.C. Feldman, Electronic Thin Film Science for Electrical Engineers and Material Scientists, Macmillian Publishing Company, New York, 1992.

[31] I. Kim, K. Uppal, W.J. Choi, and P.D. Dapkus, Composition control of InGaAsP in metalorganic chemical vapor deposition using tertiarybutylphosphine and tertiarybutylarsine, Journal of Crystal growth, (1998), vol. 193, pp. 293-299.

[32] B. Wang, F. Zhao, Y. Peng, Z. Jin, Y. Li, and S. Liu, Self-organized InAs quantum dots formation by As/P exchange reaction on (001) InP substrate, Applied Physics Letters, (1998), vol. 72, pp. 2433-2435.

[33] C.H. Li, L. Li, D.C. Law, S.B. Visbeck, and R.F. Hicks, Arsenic adsorption and exchange with phosphorous on indium phosphide (100), Physical Review B, (2002), vol. 65, DOI: 10.1103/PhysRevB.65.205322.

[34] A. Aierken, Passivation of GaAs surfaces and fabrication of self-assembled In(Ga)As/GaAs quantum ring structures, Doctoral Dissertation, Teknillinen korkeakoulu, Finland, Espoo, 2008.

[35] H. Saito, K. Nishi, and S. Sugou, Shape transitions of InAs quantum dots by high temperature, Applied Physics Letters, (1999), vol. 74, pp. 1224-1226.